COMPUTATION OF LIQUID DROPS GEOMETRY WITH MOTION OF THE CONTACT CURVES

by

Gilbert C. McCray

A thesis submitted to the Graduate College of
Texas State University in partial fulfillment
of the requirements for the degree of
Master of Science
with a Major in Applied Mathematics
August 2017

Committee Members:

Raymond Treinen, Chair

Julio Dix

Stewart Welsh

FAIR USE AND AUTHOR'S PERMISSION STATEMENT

Fair Use

Duplication Permission

ACKNOWLEDGEMENTS

There are many people who I wish to thank for getting me to this point in my academic pursuit. First and foremost, my mother, Audrey, and grandmothers Dorothy and Liz. They instilled in me a thirst for knowledge, a dedication to literacy and education, compassion, and patience. My father and grandfathers introduced me to numbers though their roles in business and church finance.

I want to also thank Dr. Freddie Frazier from Prairie View A&M University, who taught me everything from algebra to differential equations. Dr. Frazier first taught me the importance of practice, and he instilled in me as well as generations of other black STEM students the mathematical confidence to "stop playing around with the equation and just solve it". I'd also like to thank Dr. Thomas Tweed for molding me into a discerning thinker, and expanding the kinds of knowledge that I thought were valuable.

Thanks are due to my sister, Whittney, who has been filling out applications and financial aid forms for me for decades.

Special thanks to my friends, who stayed up studying with me and generally kept me from panicking over the years: Alex Milling, Prakash Ravichandar, Andy Gay, especially my research partner/friend/fellow Bobcat/father of my goddaughter Robert Shields.

Lastly, I must think my committee chair and thesis advisor Dr. Treinen for patiently guiding me through this process and gently pushing me all the way to the finish line.

TABLE OF CONTENTS

Page

LIST OF FIGURES

Figure **Page**

ABSTRACT

This paper covers the modeling of homogenous liquids adhering to a uniform solid surface. It is divided into two separate problems: the sessile drop on a horizontal plane, and the liquid bridge between two horizontal planes held apart at a fixed distance. We prove a volume formula for both problems. We use numerical methods to solve the differential equations that describe the surface of the liquid. We use a model to compute velocity along the contact line, which is the rate at which the liquid expands along the solid surface. We study the issue of the receding and advancing along the plate or plates.

I. THE STATIC SESSILE DROP

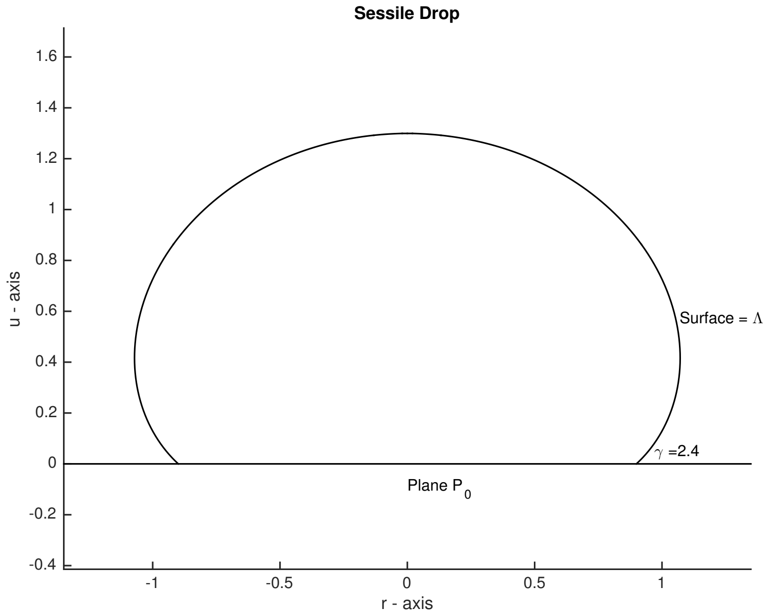

Figure I.1: A sessile drop with plane P_0 and an interfacial boundary Λ.

We consider a drop of liquid on a solid plate. Wente [10] showed that equilibrium drop shape is symmetric about a vertical axis. Thus, the sessile drop shape can be described by a radius r and a height u. It has a radius r measured from the center, where $r(0) = 0$ at the height of the sessile drop. At distance r, the liquid forms a contact angle γ between the solid plate and a surrounding fluid, which is typically air. The curve that forms the interfacial boundary between the sessile drop and surrounding fluid is parameterized by arc length s. Our construction of the sessile drop has the following initial conditions:

$$r(0) = 0 \tag{I.1}$$

$$u(0) = u_0 \tag{I.2}$$

$$\psi(0) = 0 \tag{I.3}$$

The static sessile drop surface is described by solutions to the following system of differential equations with the above initial conditions:

$$\frac{dr}{ds} = \cos\psi, \tag{I.4}$$
$$\frac{du}{ds} = \sin\psi, \tag{I.5}$$
$$\frac{d\psi}{ds} = \kappa u - \frac{\sin\psi}{r} + \lambda, \tag{I.6}$$

where u is the height, r is the radius, ψ is the angle the liquid makes with the horizontal, s is the arc length, λ is a Lagrange multiplier, and κ is a physical constant of the problem. Here, $\kappa = \rho g/\sigma$, and ρ is the density of the liquid, g is a gravitational constant, and σ is the surface tension of the liquid and air interface. In the following theorem we prove by construction that the solutions curves to (I.4) - (I.6) form an inverted sessile drop when we let $\lambda = u(\ell)$ in below.

THEOREM 1. *Let (r, u) be the generating curve of a sessile drop's liquid-air interfacial boundary. Let $u = u(s)$ and $r = r(s)$, where s is the arc length of the curve and λ is the Lagrange multiplier, then $\lambda = u(\ell)$.*

Proof. Let (r, u) be such a curve, seen in Fig I.2. Reflect (r, u) over the horizontal axis, the r-axis. This produces curve $(r, -u)$, seen in Fig I.3. Then, in order to translate the generating curve vertically so that $-u(\ell) = 0$ we add constant λ to $-u(s)$ in $(r, -u)$, which gives the curve $(r, -u + \lambda)$ (Fig I.4). Here

$$-u(\ell) + \lambda = 0 \tag{I.7}$$
$$u(\ell) = \lambda \tag{I.8}$$

$\square$

The figures below show the generating curve and how its reflected over the $r - axis$ and translated vertically.

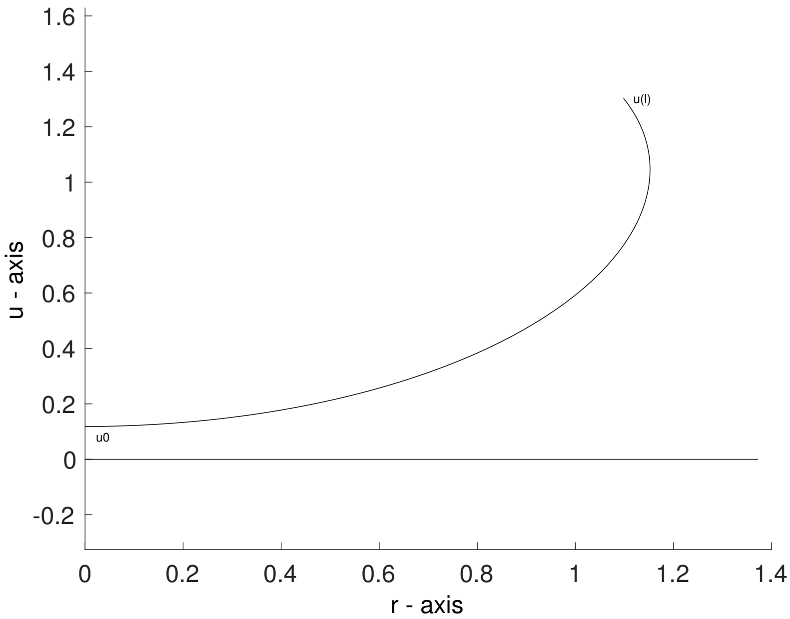

Figure I.2: A generating curve (r, u), where $u(\ell)$ is marked.

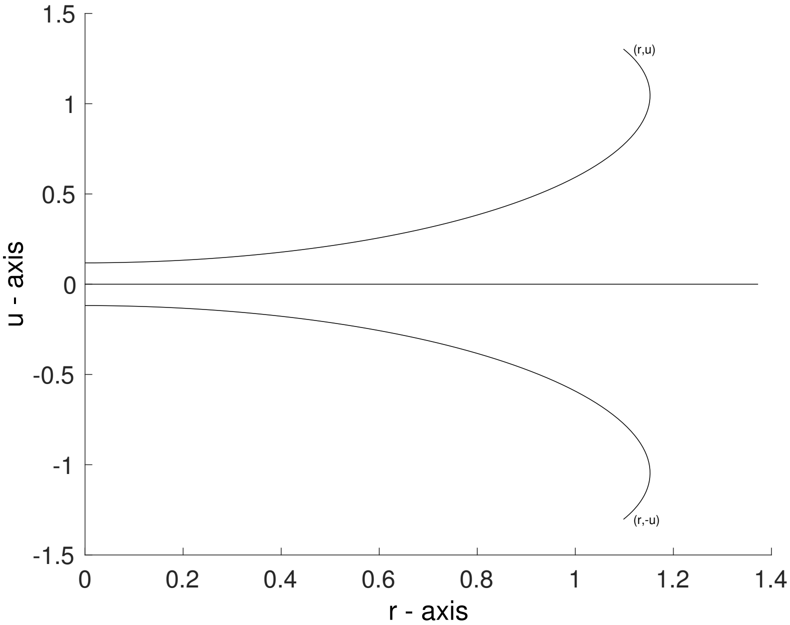

Figure I.3: A generating curve (r, u) and its reflection over the r-axis $(r, -u)$.

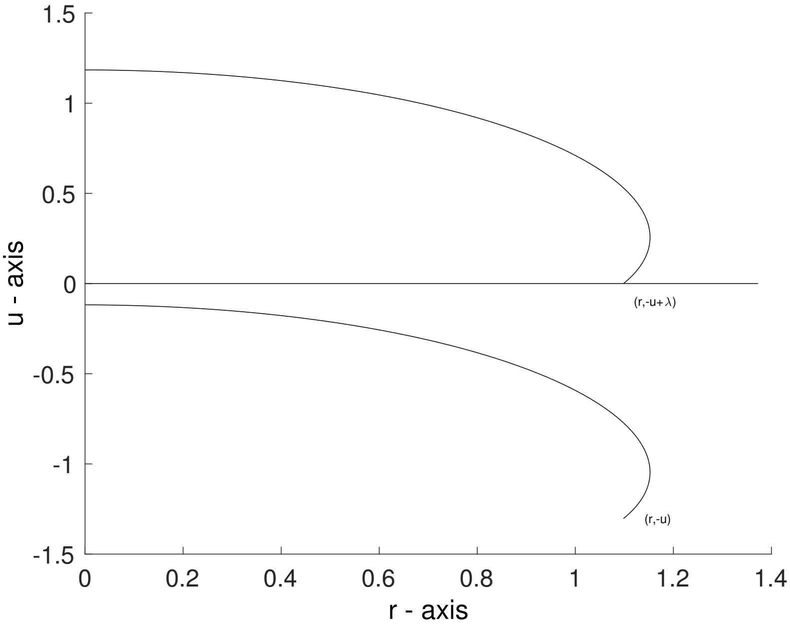

Figure I.4: Generating curve (r, u), its reflection $(r, -u)$, and the vertical translation $(r, -u + \lambda)$.

Volume of a sessile drop

The volume of the sessile drop is derived below using the initial conditions and definitions given earlier in the chapter.

THEOREM 2. *The volume of a sessile drop is*

$$V = \pi r^2 u - \frac{2\pi r}{\kappa} \sin\psi + \frac{\pi\lambda r^2}{\kappa}, \tag{I.9}$$

where (r, u) is the drop/air interfacial boundary with angle ψ.

Proof. We first integrate the volume equation by parts

$$\begin{aligned} V &= \int_0^H \pi r^2 du \\ &= \pi r^2 u - 2\pi \int_0^r \rho u \, d\rho. \end{aligned}$$

Repeated integration by parts gives that

$$\int_0^r \rho u \, d\rho. \ = \rho \sin\psi \Big|_0^r - \lambda \int_0^r \rho u \, d\rho.$$

Then we differentiate $\rho \sin\psi$ with respect to arc length s:

$$\begin{aligned}
\frac{d}{ds}\left(\rho\sin\psi\right) &= \frac{d\rho}{ds}\sin\psi + \rho\cos\psi\frac{d\psi}{ds} \\
&= \frac{d\rho}{ds}\sin\psi + \rho\cos\psi\left(\kappa u - \frac{\sin\psi}{r} + \lambda\right) \\
&= \frac{d\rho}{ds}\sin\psi + \rho\cos\psi\kappa u - \rho\cos\psi\frac{\sin\psi}{r} + \rho\cos\psi\lambda \\
&= \rho\cos\psi\kappa u + \rho\cos\psi\lambda.
\end{aligned}$$

The path along the generating curve is monotone, and we integrate with respect to s on both sides and get the result

$$\begin{aligned}
\int_0^\ell \frac{d}{ds}(\rho\sin\psi)\, ds &= \int_0^\ell (\kappa\rho u\cos\psi + \lambda\rho\cos\psi)\, ds \\
\rho\sin\psi &= \kappa\int_0^\ell \rho u\cos\psi\, ds + \lambda\int_0^\ell \rho\cos\psi\, ds,
\end{aligned}$$

where $\ell = s_{max}$. Recall $\cos\psi = d\rho/\, ds$, then

$$\begin{aligned}
\rho\sin\psi &= \kappa\int_0^\ell \rho u\frac{d\rho}{ds}\, ds \ + \lambda\int_0^\ell \rho\frac{d\rho}{ds}\, ds \\
&= \kappa\int_0^r \rho u\, d\rho \ + \lambda\int_0^r \rho\, d\rho.
\end{aligned}$$

Then

$$\begin{aligned}
\kappa\int_0^r \rho u\, d\rho \ &= \rho\sin\psi - \lambda\int_0^r \rho\, d\rho \\
\int_0^r \rho u\, d\rho \ &= \frac{1}{\kappa}\left(\rho\sin\psi - \lambda\int_0^r \rho\, d\rho\right) = \frac{r\sin\psi - \lambda r^2/2}{\kappa} \\
&= \frac{2r\sin\psi - \lambda r^2}{2\kappa}.
\end{aligned}$$

$\therefore$ The volume of a sessile drop is

$$
\begin{aligned}
V &= \pi r^2 u - 2\pi \int_0^r \rho u \, d\rho \\
&= \pi r^2 u - 2\pi \left(\frac{2r \sin\psi - \lambda r^2}{2\kappa} \right) \\
&= \pi r^2 u - \frac{2\pi r}{\kappa} \sin\psi + \frac{\pi \lambda r^2}{\kappa}.
\end{aligned}
$$

$\square$

Numerical Solver

In *Equilibrium Capillary Surfaces*, Finn [3] holds that volume $\mathcal{V}$ is a continuously differentiable function of energy u_0 and proves that there is a unique solution for a given contact angle γ. The solution to the sessile drop problem is divided into two approaches. The first approach is when given a fixed volume V_0 and contact angle γ, then one can solve for radius r. Alternatively, when given fixed volume V_0 and fixed radius r, then we calculate the contact angle $\psi(\ell)$.

In this section we will established that the solution exists for a fixed volume liquid drop, called a *static sessile drop*. We will later demonstrate its robustness, with solutions for any volume, assuming that the radius and contact angle are selected appropriately. Note that Finn's theorem guarantees a unique contact angle $0 < \gamma < \pi$ for some $\mathcal{V} > 0$. For the sessile drop of variable volume over time, we have similar cases at each time step. Below, we discuss the numerical methods developed for generating the interfacial boundaries of the sessile drop and the solutions for a given volume.

We use a shooting method to find solutions to the three differential equations (I.4) - (I.6). This is a two-point boundary problem with boundary conditions $\psi(0) = \gamma$ and $\psi(\ell) = \gamma$. We implement two nested algortihms, an inner implementation of an adaptive Runge-Kutta-Felberg method and an outer implention of a multidimensianal root finder as used by Colter and Treinen in *Cylinderical Liquid Bridges* [2].

Values for either γ or r, along with $\mathcal{V}$ and u_0 are prescribed for the desired solution. The initial conditions for the boudnary value problem are given by (I.1) - (I.3) and our terminating conditions are given below:

$$r(\ell) = r \tag{I.10}$$

$$u(\ell) = \lambda \tag{I.11}$$

$$\psi(\ell) = \gamma \tag{I.12}$$

where the ending arc length ℓ is chosen to terminate at $u(\ell) = \lambda$ with the tangent to the curve forming the angle γ with the solid surface.

The boundary value problem is also solved using a shooting method used by Colter and Treinen [2]. The solver uses the adaptive Runge-Kutta-Felberg method for 4th and 5th order, implemented by MATLAB as ODE45. Tolerance was set to $1e - 8$. To begin to solve the problem, reasonable guesses are given for the free parameters: the radius of our curve r, the arc length ℓ, and the Lagrange multiplier λ.

We begin by guessing suitable values for unknowns $\mathbf{guess} = \langle \ell, u_o, \lambda \rangle$. The guess parameters are adjusted in the multidimensional root finder in MATLAB called FSOLVE. We set the tolerances for this portion to $1e - 6$. This generates solutions to our system of differential equations (I.4) - (I.6) with new values of the parameters r, ℓ, and λ at each step, until (I.10) - (I.12) are satisfied to the prescribed tolerance. These values are used to generate candidates satisfying the ODE. Then the solutions to (I.4) - (I.6) with these values of the free parameters are used to evaluate the equations below:

$$V = V_0, \tag{I.13}$$

$$\psi(\ell) = \gamma, \tag{I.14}$$

$$u_0 = \lambda, \tag{I.15}$$

where V_0 is a given volume, and γ is the contact angle for a particular system. FSOLVE adjusts the parameters r, ℓ, and λ. At each step, new solutions are generated, which are then evaluated by ODE45. Once the residuals (I.13) - (I.15) are solved to within our tolerance, then the static problem is solved. We consider the problem solved when our ending conditions are satisfied.
Note: Capillary_ODE_Solver is our solver. ResFun is our rootfinder, where *Res* means residuals.

Sessile Shapes and dependence on γ

There should exist a sessile drop with some $\gamma \in (0, \pi)$ for every volume $\mathcal{V} > 0$ [3]. Below in Fig. I.5 - Fig. I.7, we see six sessile drops ranging from γ slightly above zero to $\gamma \approx \pi$. They are all of the same volume. Uniqueness demands that for a given prescribed contact angle γ, there should be a unique radius. We see that there is a solution for the full range of possible angles, and how the radius changes with γ input as expected.

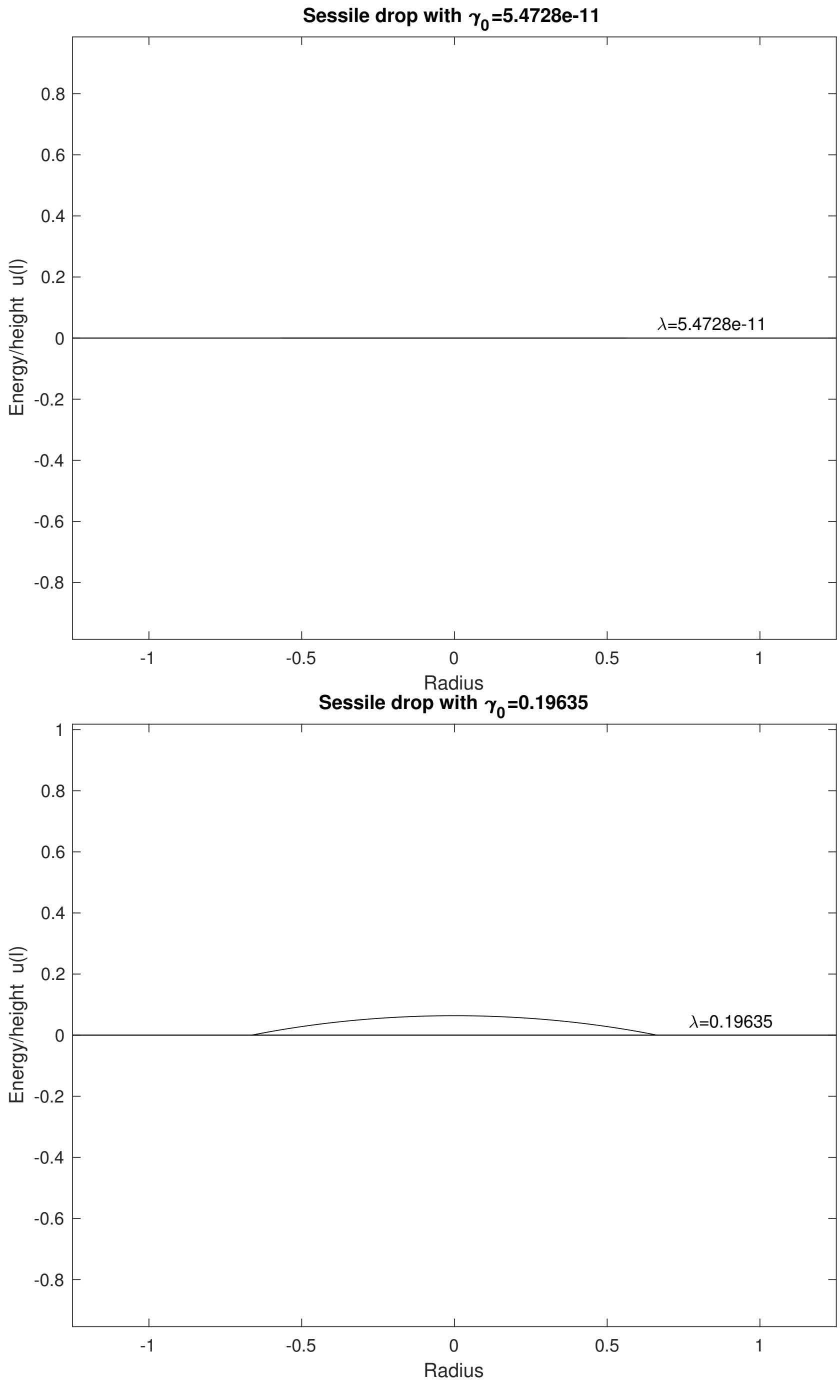

Figure I.5: Sessile drop examples with volume $\gamma \approx 0$ and $\gamma = 0.19635$.

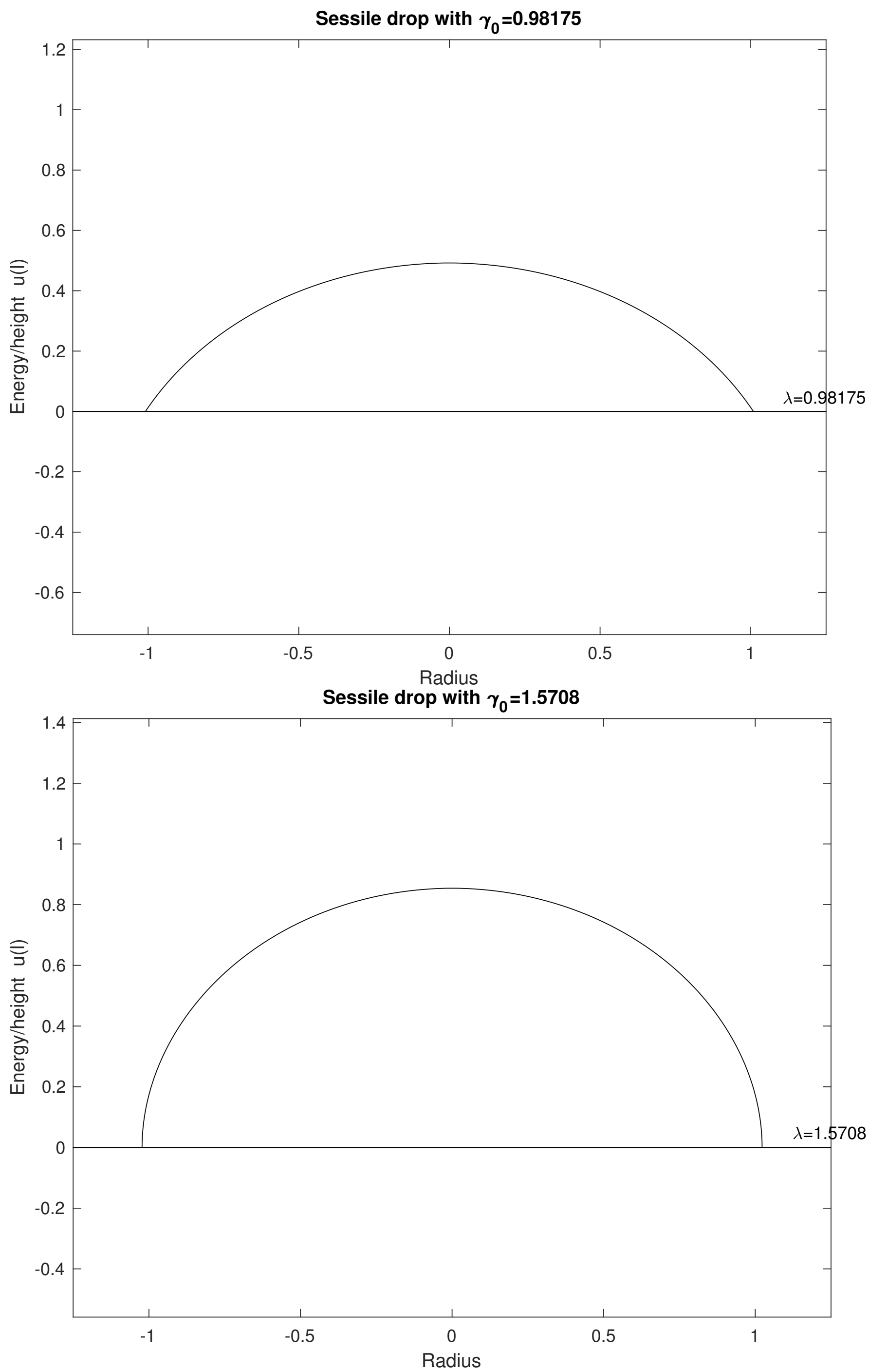

Figure I.6: Sessile drop examples with volume $\gamma = 0.98175$ and $\gamma = \pi/2$.

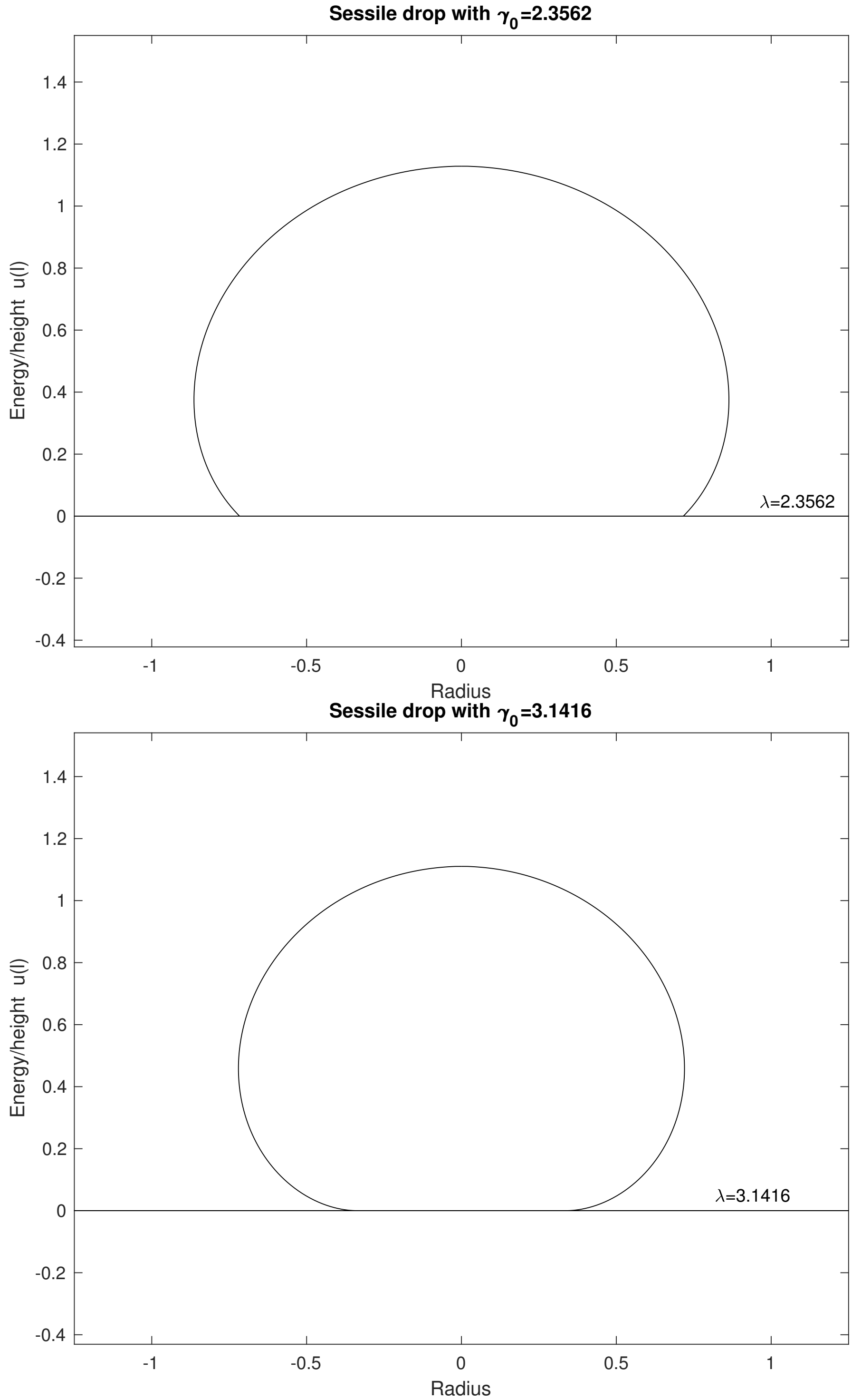

Figure I.7: Sessile drop examples with volume $\gamma = 2.3562$ and $\gamma \approx \pi$.

II. THE DYNAMIC SESSILE DROP

We may allow that the contact angle γ vary over time. For the dynamic problem we calculate $\psi(u,t)$. In doing so we may or may not find an equilibrium position for r or ψ, even though theoretically a sessile drop of volume $\mathcal{V}$ should exist for some ψ, when r is free. Our main investigation in this chapter is to calculate the velocity of the contact line $v(t)$ for different volume inputs. We will vary our volume equations $V(t)$ (e.g. constant, sinusoidal, logarithmic, or exponential), and similarly we explore the various friction scenarios along the contact line with friction coefficient κ_S.

Accurately describing the friction equation κ_S is the problem of finding the coefficients of friction and slip of a liquid moving atop a solid surface and combining them. This has been a challenge for about a century. In *Hydrodynamic model of steady movement of a solid/liquid/fluid contact line*, Huh and Scriven [7] considered the problem of a liquid drop to be one liquid and a lubricating medium, a second immiscible fluid in between the first liquid and a solid surface. Here the drop itself is the lubricating fluid for air (the liquid) in the conventional model. They concluded that intermolecular forces are the primary driver of contact line movement. In his paper *On the motion of a small viscous droplet that wets a surface*, [5] finds that

$$\kappa_S(h) = \frac{\alpha}{3h}, \tag{II.1}$$

which he derived based on methods used by [7], where α is small to reflect the small height for Greenspan's model of a very short yet widespread sheet of liquid. He found

$$v(t) = \kappa_s(\theta - \theta_S), \tag{II.2}$$

where θ_S and θ are the static and dynamic (observed) contact angles, respectively.

Early on it was believed that the internal flow of the fluid is the primary driver inside the drop Finn and Shinbrot [4]. However, it was later discovered visually that movement of the contact line along the solid surface happens in a more stop-gap manner due to nonconformity at the molecular level. Finn and Shinbrot explore *stick-slip motion* and how it describes movement of liquid along a horizontal plane Finn and Shinbrot [4]. Visual methods were used to precisely measure the slip coefficient κ_S, which is function that captures the molecular forces in between the liquid and the flat solid, as well as at the boundary between the surface of the liquid, air, and solid.

We assume that friction holds the drop in place for some time, and then sets a shape with a radius r and contact angle γ. If the sessile drop finds a stable configuration at this radius, where changes in γ are negligible, then we have an equilibrium. But, if we are not at an equilibrium contact angle, $\psi(\ell)$ increases towards π, and once the contact angle exceeds π, the wetted region no longer contains the volume, and the wetted area increases. They concluded that intermolecular forces are the primary drivers of movement.

Huh and Scriven Huh and Scriven [7] call this *dynamic wetting.* That is to say wetting with a dynamic contact angle, a problem currently under investigation. Typically, for a given contact angle γ, there is a wetted region of some area, with drops wetting that region up to a maximum volume. Once this volume is exceeded, the wetted region must expand. This forms the basis of a model that is a hybrid of the static and dynamic problems. The movement of the contact line is measured by expansion of the wetted region. The velocity of the contact line is expected to go to zero, and given a static volume the drop settles into an equilibrium. However, for changing volume, the system will never find an equilibrium. Further, the velocity of the contact line, as we will show is expected to be a continuous function of time.

Velocity

The static velocity equation for the contact line or *contact velocity* is given by Guidotti in *Equilibria and Their Stability for a Viscous Droplet Model* Guidotti [6] as

$$v(|\nabla u|) = |\nabla u|^2 - 1 \text{ or } v(|\nabla u|) = |\nabla u|^3 - 1.$$

This velocity is determined the physical parameters of a static Sessile drop, and is determined by the type of liquid and solid we have. However, we cannot easily calculate ∇u. Note that $\nabla u = \tan\psi \approx \psi$ for small ψ, and since $\psi, \gamma > 0$, then $|\psi - \gamma| \ll \pi$. Note that because $\lim_{\psi\to\pi/2}(\tan\psi)$ is undefined, we cannot use $\tan\psi$ in our velocity function. Thus, we approximate the contact line's velocity as

$$v(\psi, \kappa_S, \gamma) = \kappa_S(\psi - \gamma)^2 \tag{II.3}$$

or

$$v(\psi, \kappa_S, \gamma) = \kappa_S(\psi - \gamma)^3, \tag{II.4}$$

where κ_S is a slip function for the interfacial friction between liquid and solid and γ is the contact angle.

Utilizing the Euler Method, we get the radius $r(\ell, t)$ as a function of velocity $v(\ell, t)$ at time t. This method recalls our previous solver functions, and we calculate $r(s, t)$ at $s = \ell$ and $r(t)$ below

$$\begin{aligned} r(0,t) &= \Delta t\left(\frac{d}{dt}r(\ell,t)\right), \\ &= \Delta t\left[v(\psi(\ell,t),\kappa_s,\gamma)\right], \\ &= \Delta t\left(\kappa_S(\psi(\ell,t)-\gamma)^3)\right). \end{aligned} \tag{II.5}$$

The algorithm for the contact velocity shown in Appendix A, and here $\Delta t = 0.001$ for the sessile drop simulations.

Steady state solution

Here we look for a dynamic system that falls into an equilibrium. We consider the system in equilibrium is when the velocity goes to zero and the contact radius remains in place. Sufficient conditions in our model are when $v(t) < \epsilon$ and $\Delta v(t) < \epsilon$ for some tolerance ϵ over a given amount of time. Arbitrarily we choose $\epsilon = 5e - 5$ over 10 timesteps, $\Delta t = 0.01$.
We calculate the equilibrium γ using the previous method for finding γ, given a radius r_0 with the following ending conditions being met:

$$V = V_0, \tag{II.6}$$

$$r(\ell) = r, \tag{II.7}$$

$$u(\ell) = \lambda, \tag{II.8}$$

where r is again calculated using the Euler method, and we generate a new sessile curve for each time step.

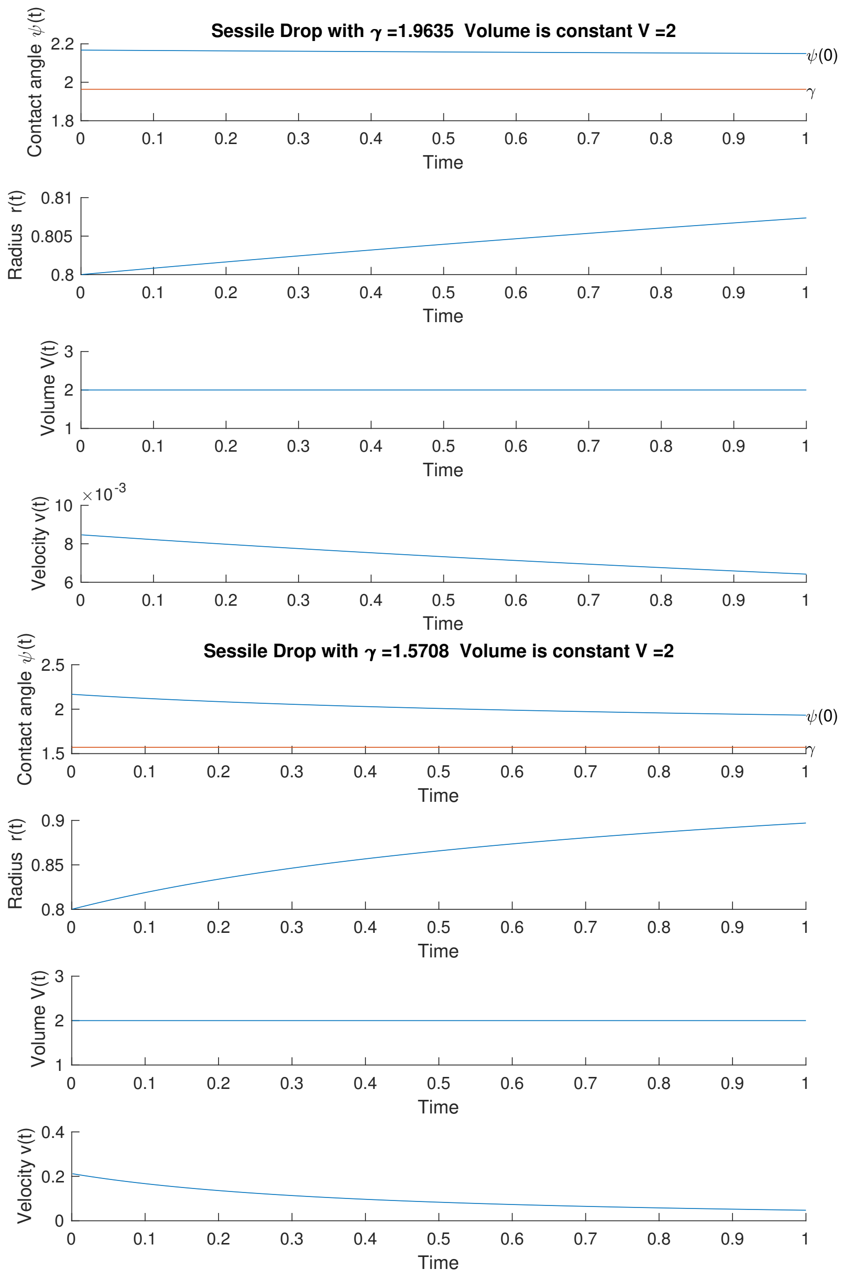

Figure II.1: Two dynamic sessile drops with constant volume.

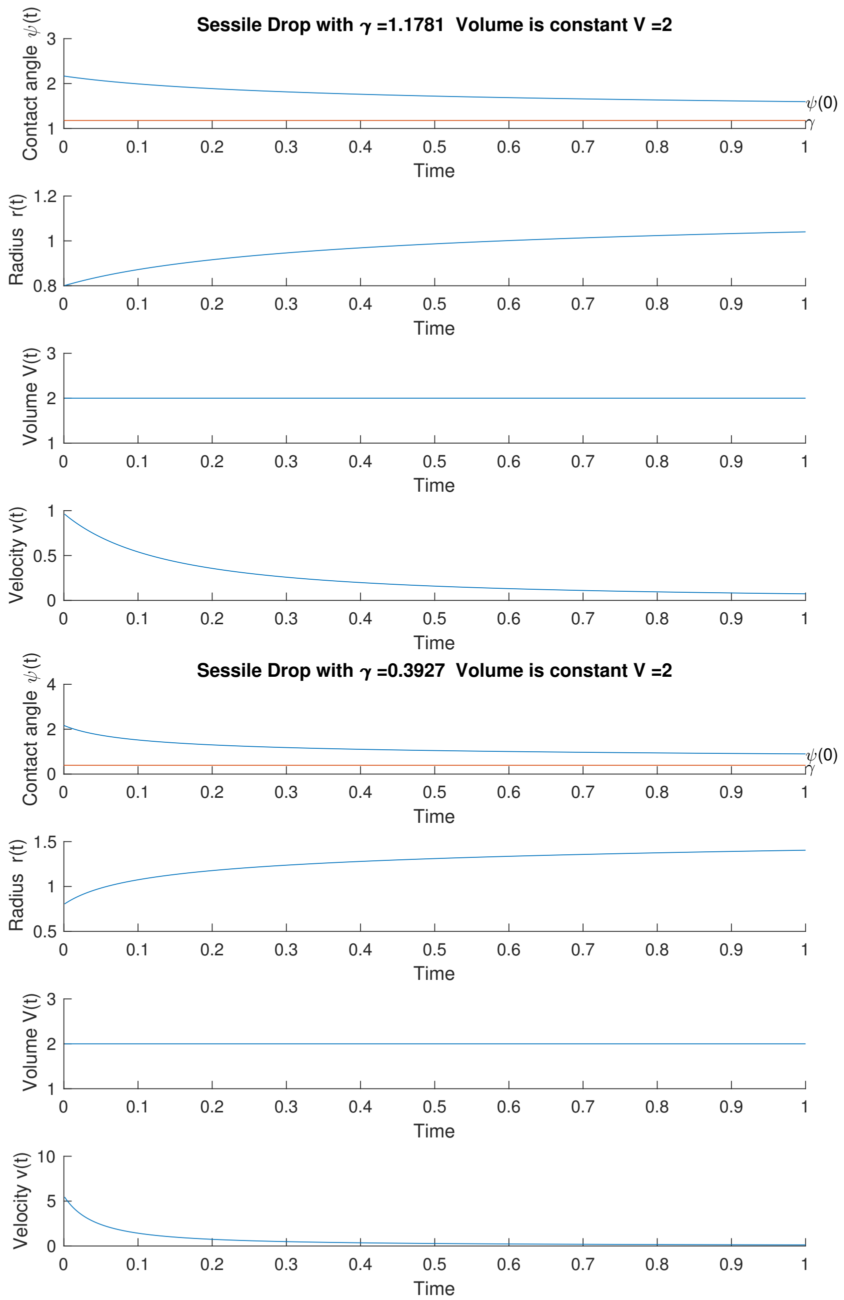

Figure II.2: Two dynamic sessile drops with constant volume.

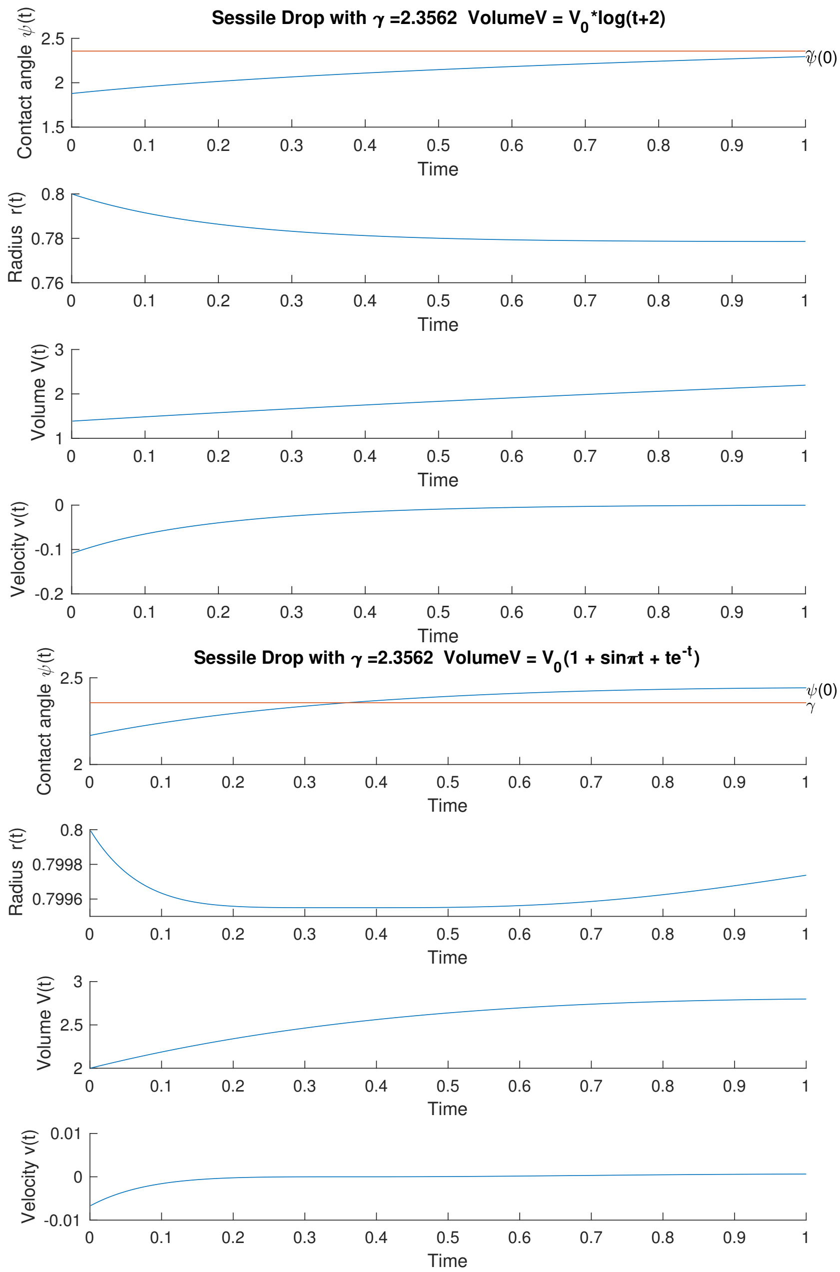

Figure II.3: Two sessile drops with velocity heading towards zero.

For a dynamic sessile drop with static volume we expect to find examples where as $v \to 0$ then $\Delta r = 0$. This is the equilibrium solution for the dynamic model, where $\psi(\ell)$ moves towards an equilibrium contact angle for a given volume $\mathcal{V}$ and radius r as seen in Fig. II.1 and Fig. II.2.

Given variable volume we expect the system to fall into a dynamic equilibrium, where velocity of the contact line does not change. In this state ψ will not change as seen in Fig. II.3. Consequently, so does the contact angle γ. We conclude that the dynamic sessile drop with variable volume is computationally the same problem, however, the velocity never reaches zero while volume changes.

To test these ideas, we considered a volume function $V(t)$ that does not tend any value

$$V(t) = V_0 \left(1 + \sin(\pi t) + te^{-t/h}\right), \tag{II.9}$$

where V_0 is the initial volume. The timestep h is set at 0.001 to ensure that volume does not change to quickly and we get a smooth velocity function, shown below in Fig. II.4.

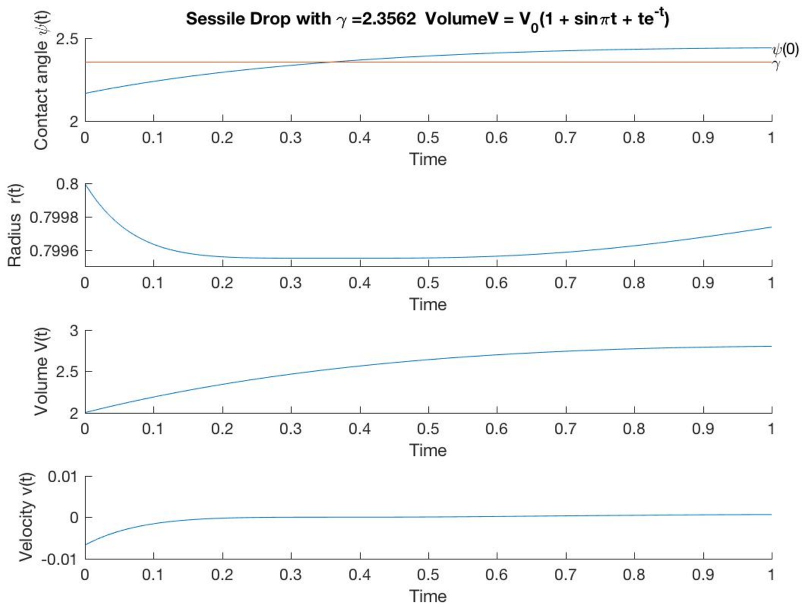

Figure II.4: A sessile drop with an increasing volume function and contact angle $\gamma = 2.3562$.

Non-equilibrium solution

We also evaluated the problem where volume greatly increases over time $t = 1$. We see in Fig. II.5 that velocity does tend towards a value, but since it is non-zero, the radius expands, and the drop grows continually. This is a non-equilibrium solution. Another example is the temporary equilibrium that we see in Fig. II.6. This is when velocity does equal zero after some time, but then as volume increases, the radius continues to grow. Notice that in Fig. II.6, while velocity is near zero that $\psi(\ell) \approx \gamma$, when $t \approx 0.5$. This is due to the rapid rise in volume, which nearly triples in our timeframe, driving a change in $\psi(\ell)$, while $\Delta r \sim 0$ remains relatively unchanged. As expected velocity is positive because $\psi(\ell) > \gamma$ near $t = 0.5$. In Fig. II.7 we see that the velocity initiates near $v \approx 0$ as $\psi(\ell) \approx \gamma$ at $t = 0$. However, we see after $t > 0$, velocity continually increases, and an no point seems to tend towards any value. This is another example of a non-equilibrium solution.

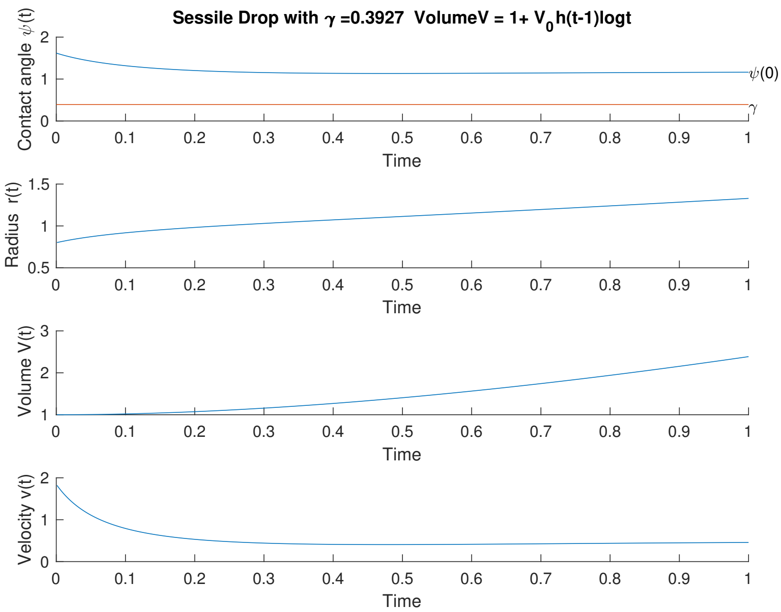

Figure II.5: A dynamic sessile drop run with $\gamma = 0.3927$ and logarithmic volume. Velocity tends to zero, while volume increases.

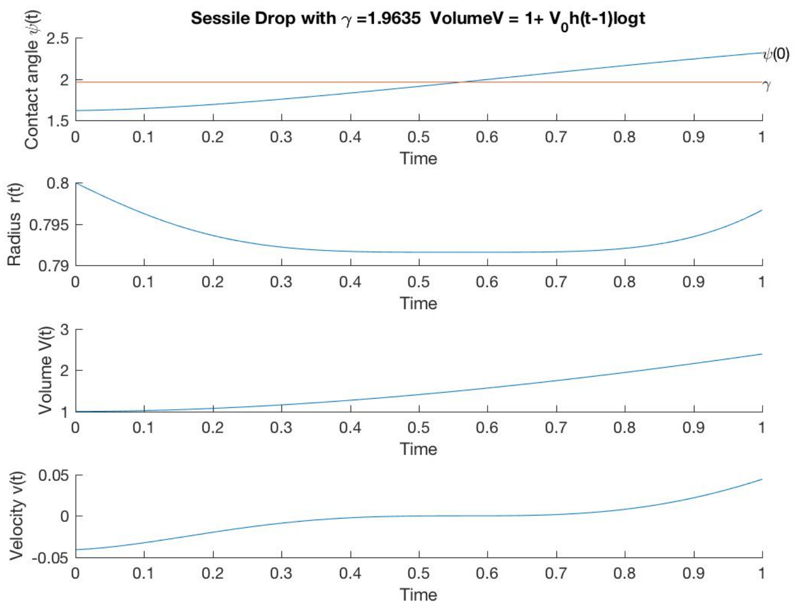

Figure II.6: A dynamic sessile drop run with $\gamma = 1.9635$ where velocity briefly plateaus then increases after time, while velocity increases.

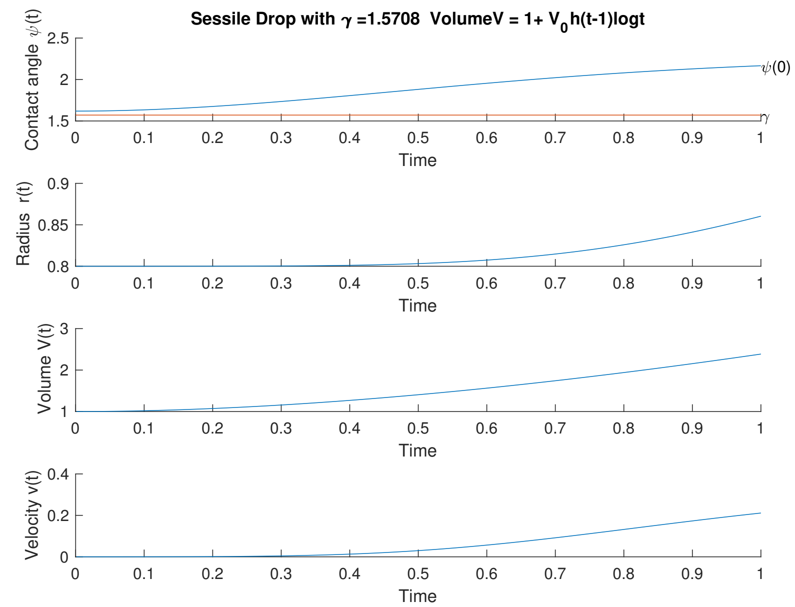

Figure II.7: A dynamic sessile drop run with $\gamma = 0.3927$ and logarithmic volume. Velocity tends to zero, while volume increases.

III. THE RECEDING AND ADVANCING ANGLES OF THE SESSILE DROP

From physical observation we know that there is an interval of contact angles $\theta_R \leq \psi(\ell) \leq \theta_A$, between which contact angle $\psi(\ell)$ has solutions to the sessile drop for radius r. This range determines an equilibrium region (E_R) for a given radius r. [8] assert that this range is actually caused by molecular imperfections and the friction created though contact line movement at the molecular level, whereas Finn and Shinbrot Finn and Shinbrot [4] claim that this is actually an equilibrium region of contact angles, where presumably we could say that $E_R = [\theta_A, \theta_R]$ for a given radius r, where the drop will not change but the contact angles are not static. When the contact line has velocity $v_0 \neq 0$, $\Delta\gamma \neq 0$ because of velocity equation. However, because of the equilibrium region when $\theta_R \leq \gamma \leq \theta_A$, we can expect that $\Delta r = 0$.

In the physical interpretation this means that while $\psi(\ell) \in [\theta_R, \theta_A]$, the radius will stand still. Then the sessile drop will become more bulbous or more flat while the contact line remains still, until the angle reaches a critical value its maximum value for the wetted region. Then the radius will either increase or decrease to maintain the stability of the drop. The difference between the advancing and receding angles, $\mathcal{H} = \theta_R - \theta_A$, is called the *contact angle hysteresis*. There are inconsistencies in any surface that cause sudden pressure drops and extreme changes in friction across very short distances. This concept is more naturally understood while observing a variable volume model, because the radius would be moving. Thus, the contact line would move across these pressure gradients and variable friction areas. However, it should also work with a static volume given a nonzero velocity, even though with static volumes the sessile drop quickly reaches an equilibrium so that effectively $\Delta r \to 0$ after some time t. We shall model the situation with both static and variable volume below.

Guidotti gives two possible contact line velocity equations

$$v = |\nabla u|^3 - 1 \text{ or } v = |\nabla u|^2 - 1.$$

We modified the squared and cubed terms to use our unknowns, which are important positions for $\psi(s)$: (1) ψ, the contact angle, (2) θ_R, the receding angle, and (3) θ_A, the advancing angle, where

$$v \sim \pm\kappa_S(\psi - \theta)^3, \text{ or} \tag{III.1}$$

$$v \sim \pm\kappa_S(\psi - \theta)^2. \tag{III.2}$$

While modelling the sessile drop, we found that the cubed velocity equation (III.1) is preferable. It changes slowly and better ensures smoothly changing contact angles. Similar to Finn and Shinbrot, we use a stop-and-go velocity, in the piecewise function below, where velocity is negative when $\psi(\ell) < \theta_R$, and we need the radius to shrink, or velocity is positive and we want radius to grow, when $\psi(\ell) > \theta_A$, otherwise velocity is zero, and given by:

$$v = \begin{cases} \kappa_S(\psi(\ell) - \theta_A)^3 & \text{when } \psi(\ell) > \theta_A, \\ -\kappa_S(\theta_R - \psi(\ell))^3 & \text{when } \psi(\ell) < \theta_R, \\ 0 & \text{when } \psi(\ell) \in [\theta_A, \theta_R]. \end{cases} \tag{III.3}$$

From (III.3), we can see that as $\psi(\ell) \to \theta_A$ or $\psi(\ell) \to \theta_R$, then $v \to 0$, and we expect that without setting $v = 0$, we would never reach equilibrium as we saw often in the dynamic sessile case.

A sinusoidal volume function is probably the best visual representation of zeroed velocity as $\psi(\ell) \to \theta_R$ or $\psi(\ell) \to \theta_A$. While $\psi(\ell) \in [\theta_A, \theta_R]$, it is clear that when $v \equiv 0$, then r is constant. We see this beow in Fig. III.1.

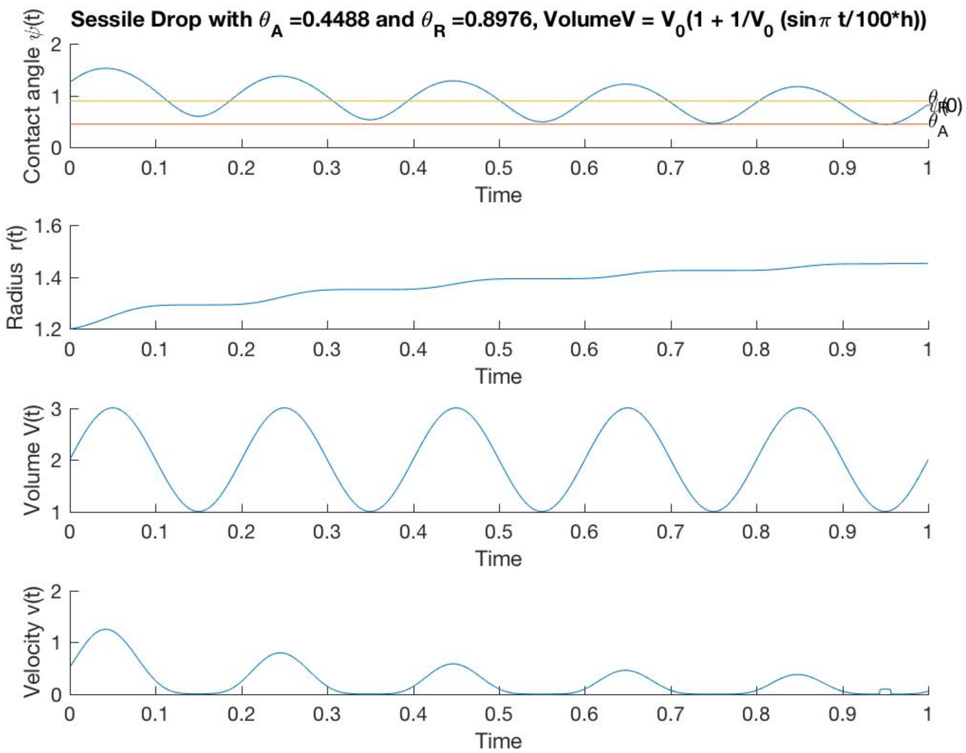

Figure III.1: An advancing and receding angle model sessile drop with sinusoidal volume.

In Fig. III.2 we see a constant volume function with expected behavior where as $\psi(\ell)$ trends toward θ_R, velocity moves smoothly to zero. Here movement is mostly determined by the angle dependent velocity term where radius is pushed out to decrease the contact angle, this is flattening of the drop.

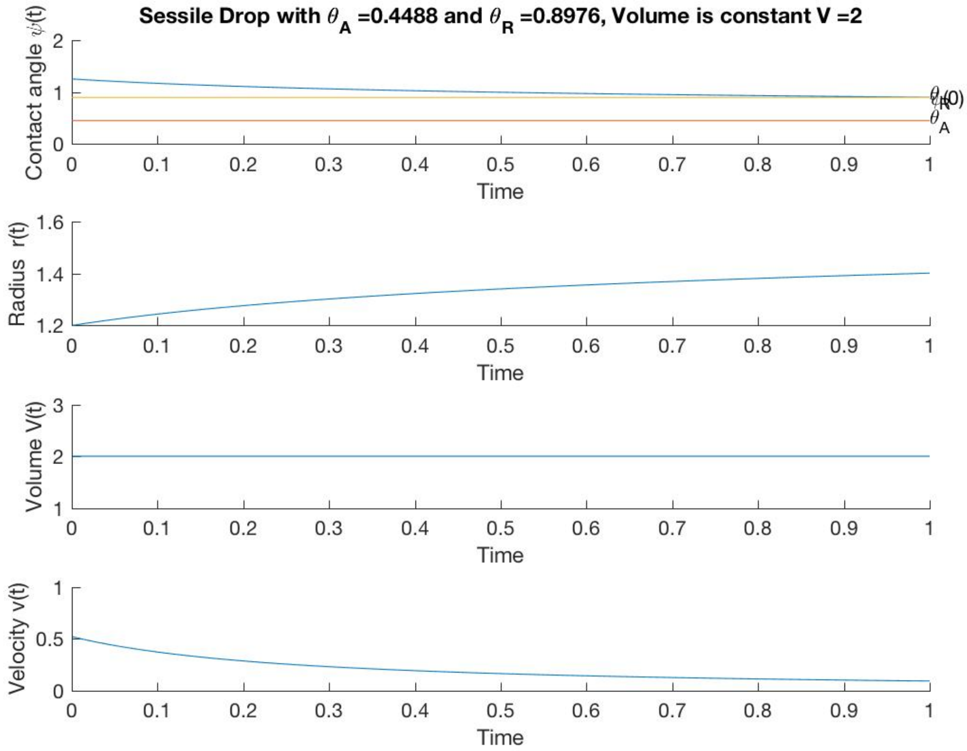

Figure III.2: A sessile drop with advancing angle $\theta_A = 448799$ and receding angle $\theta_R = 8975979$.

IV. CONCLUSIONS FOR SESSILE DROPS

The observed robustness of the sessile drop is due in part to Finn's uniqueness theorem for the sessile drop Finn [3], where a solution should always exists for any Volume $\mathcal{V}$, and in part to the success of the solver code. As we will see in the liquid bridge section this is not always a given. We see as $\psi(\ell) \to \gamma \in (0, \pi]$ that solutions always exists, as predicted. However, ubiquitous solutions did not guarantee an equilibrium solution in the dynamic sessile model. From graphical analysis from below, velocity seems heavily dependent upon volume, and we can conclude that any $\Delta V > 0$ creates either a new contact angle γ or new radius r_0. In the advancing and receding angles analysis, this is shown clearly, while $v = 0$ and $\Delta r = 0$.

Equilibrium contact angle

Observing the sessile drop with constant volume over different values of γ, an interesting trend emerges in velocity. Velocity goes from negative to nearly zero to positive.

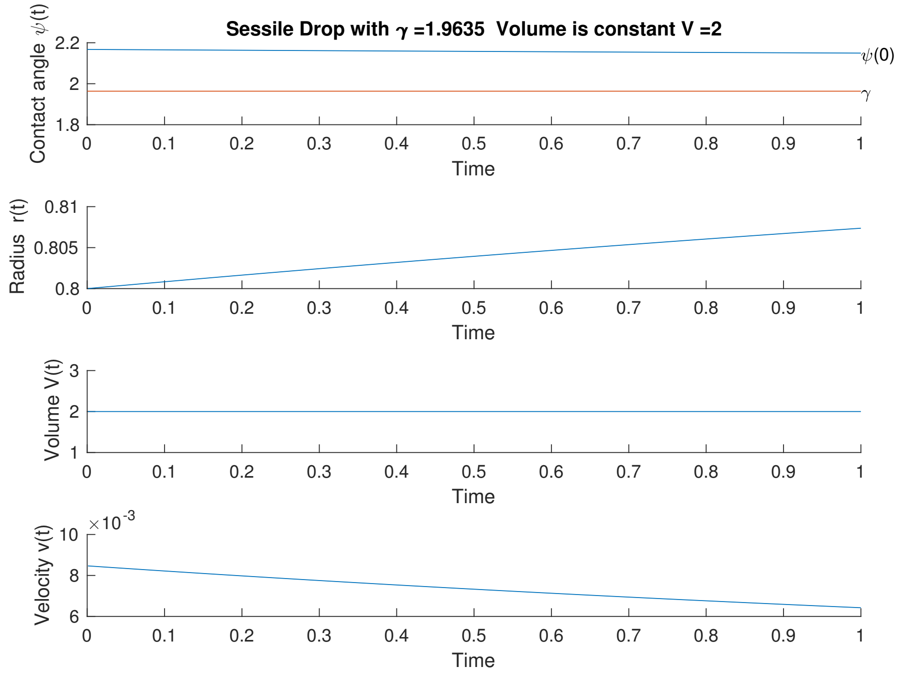

Figure IV.1: A dynamic sessile drop with constant volume, with $\gamma = 1.9635$.

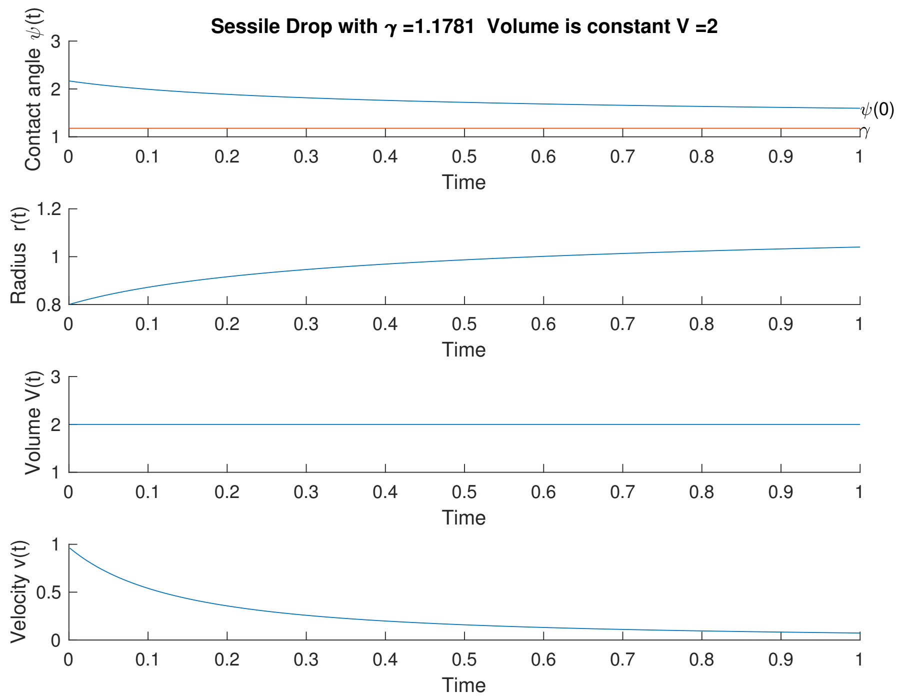

Figure IV.2: A dynamic sessile drop with constant volume, with $\gamma = 1.1781$.

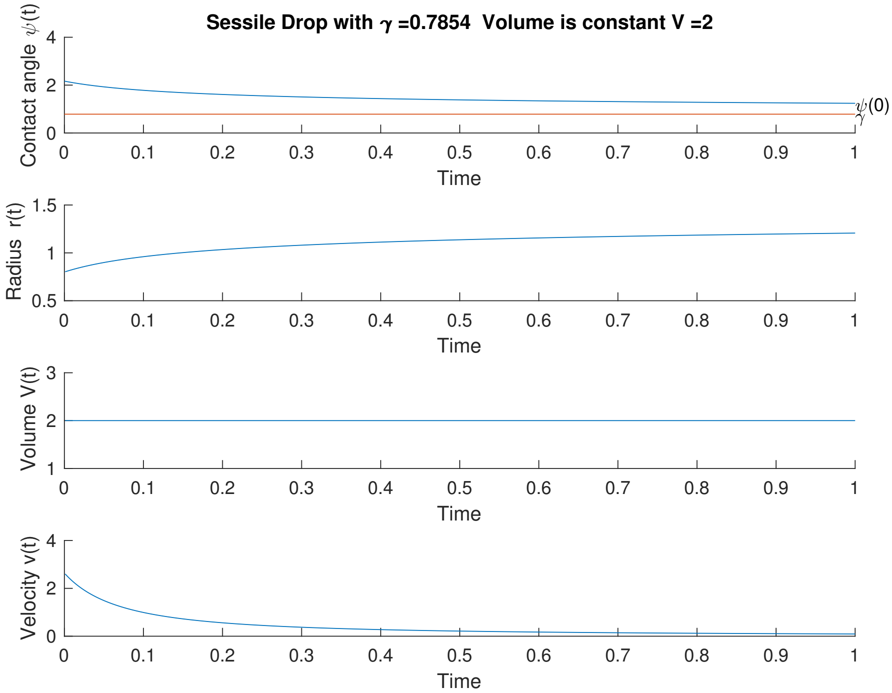

Figure IV.3: A dynamic sessile drop with constant volume, with $\gamma = 0.7854$.

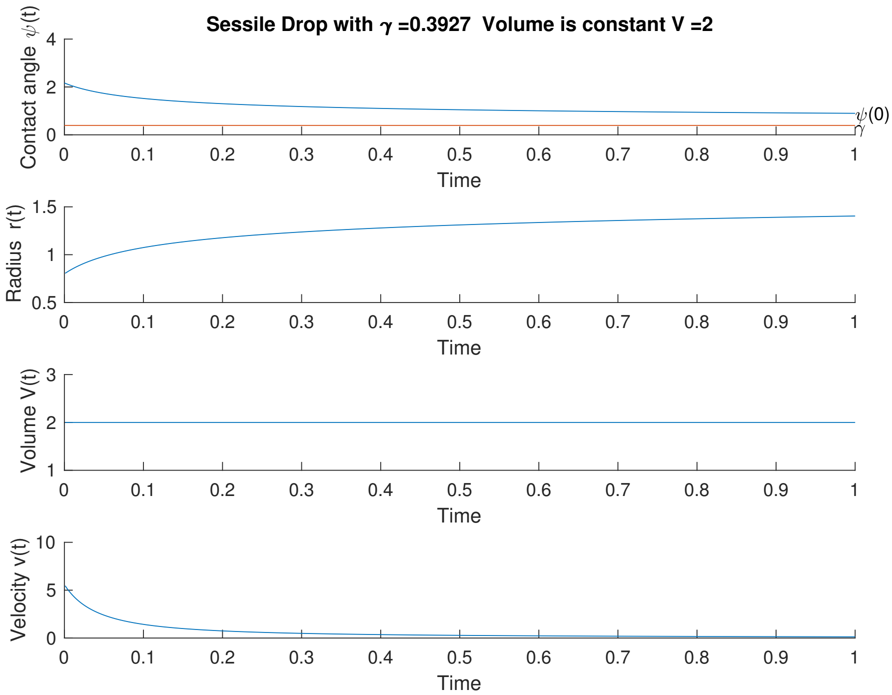

Figure IV.4: A dynamic sessile drop with constant volume, with$\gamma = 0.3927$.

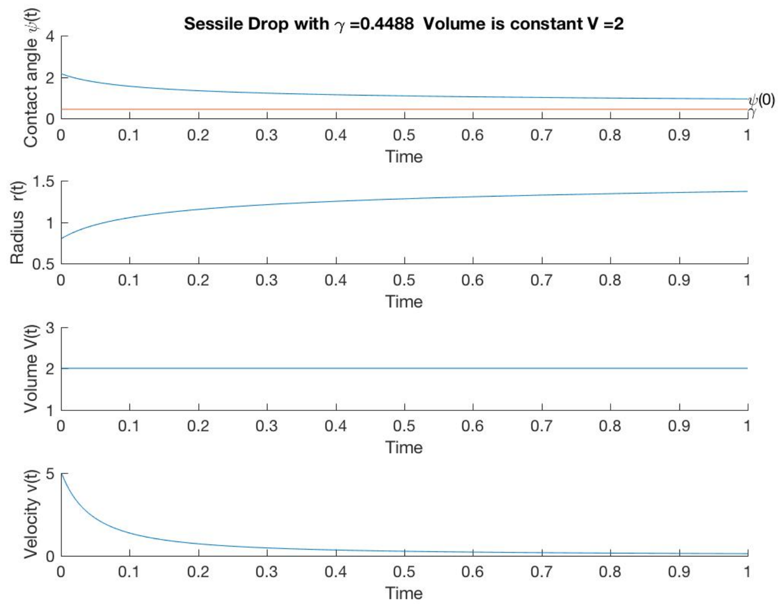

Figure IV.5: A dynamic sessile drop with constant volume, with $\gamma = 0.4488$.

And, below we see negative velocities.

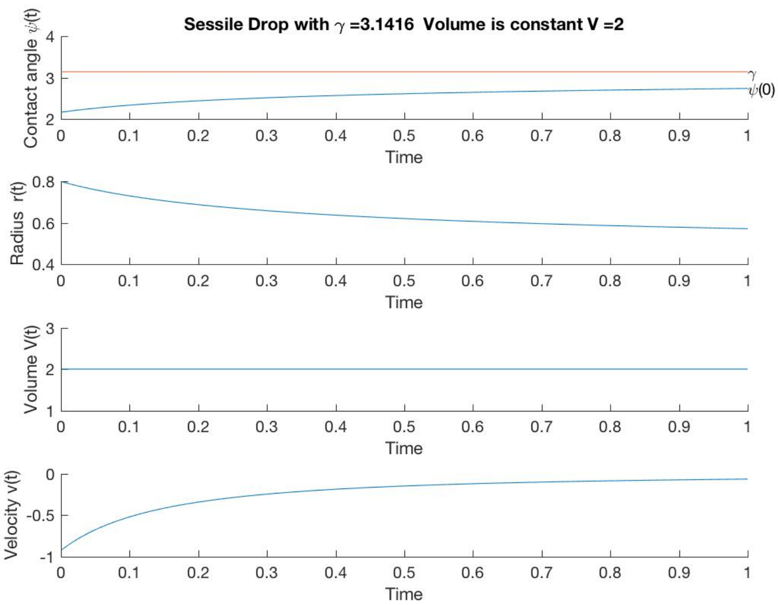

Figure IV.6: A dynamic sessile drop with constant volume, with $\gamma = 3.1416$.

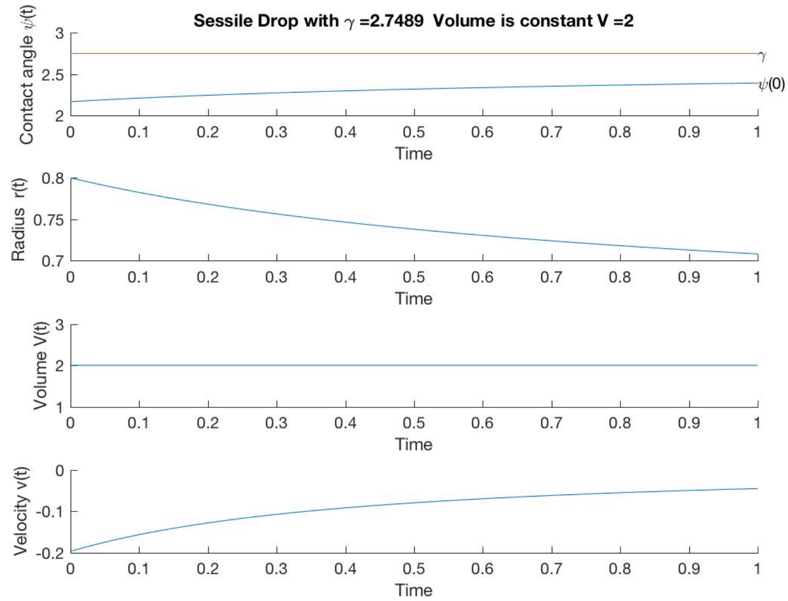

Figure IV.7: A dynamic sessile drop with constant volume, with $\gamma = 2.7489$.

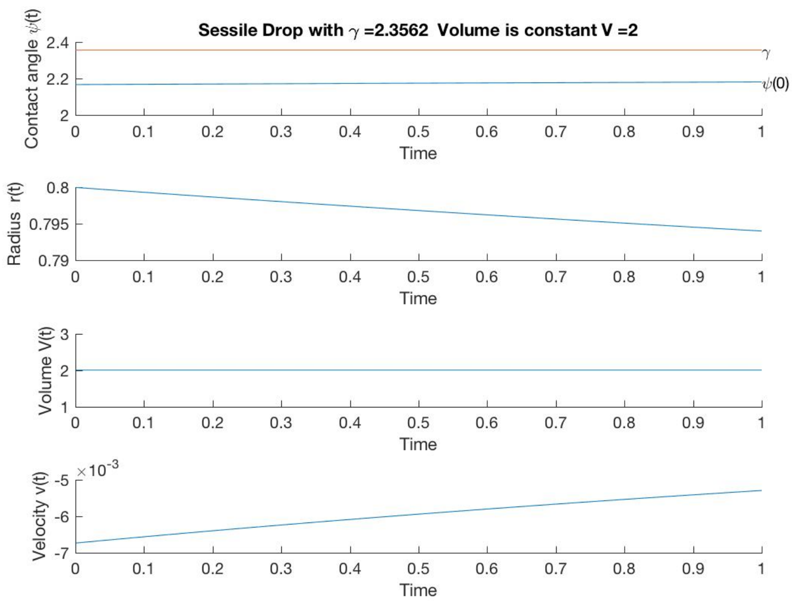

Figure IV.8: $\gamma = 2.3562$

From the above, Fig. IV.1 - Fig. IV.8, we might infer that a natural contact angle for this $(V) = 2$ is in between $\gamma = 1.9635$ and $\gamma = 2.3562$, because the velocity stays near zero for both, and the velocities are negative for $\gamma \geq 2.3562$. This could also hint at an equilibrium region E_R.

Further, comparing $\psi(\ell)$ behavior to what we calculated in the advancing and receding angles simulation, we see compelling evidence for heavy volume dependence of ψ. The graphs below show that $\psi(\ell)$ changes inside of the hysteresis region even while velocity $v = 0$. A sinusoidal volume function on a dynamic sessile drop simulation demonstrates $\psi(\ell)$ behavior in Fig. IV.9.

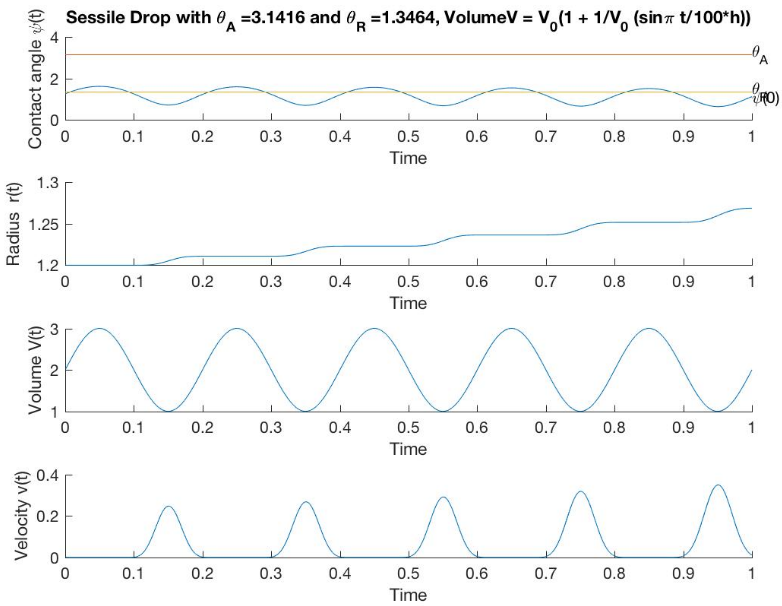

Figure IV.9: An advancing receding angle sessile drop with sinusoidal volume.

One issue with our $v = \kappa_S(\gamma - \theta_A)^3$ and $v = -\kappa_S(\theta_R - \gamma)^3$ velocity functions can be asymptotic under slowly changing volume. In Fig. IV.10 we see $\psi(\ell)$ start below θ_A. Outside of the hysteresis region, velocity is designed to move the contact line to get $\psi(\ell)$ to move into the hysteresis region by either being positive or negative. This however forms an asymptotic relationship because $\theta \to \gamma$ as $(\theta - \gamma)^3 = v \to 0$ faster.

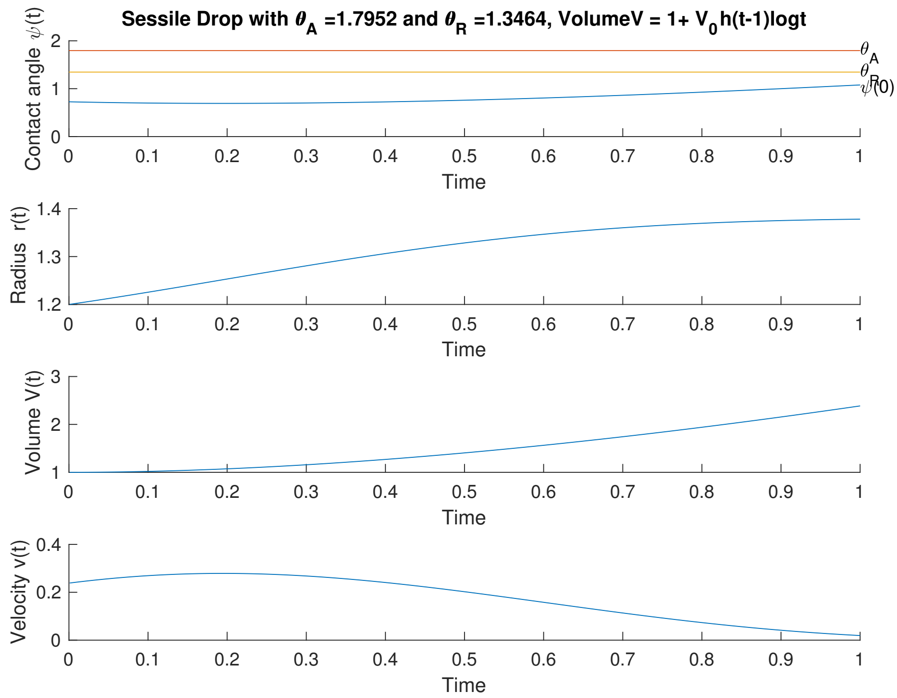

Figure IV.10: An advancing and receding model sessile drop with log volume where $\psi(\ell)$ never crosses θ_A before $v = 0$.

Failures

There was really only one consistent source of failure in the sessile advancing and receding angles model. In instances where the contact angle $\psi(\ell)$ at $t = 0$ was significantly less than θ_A or when $\psi(\ell)$ is much lower than θ_A or much higher than θ_R. We see discontinuities in velocity and along the $\psi(\ell)$ curves.

V. THE STATIC LIQUID BRIDGE BETWEEN TWO HORIZONTAL SURFACES

In this chapter we consider the liquid bridge, a radially symmetric volume of liquid between two horizontal planes, P_0 and P_H. P_0 is at height $u(0) = 0$. At the interfaces between the horizontal planes and the liquid both have the same considerations as the solid in the sessile drop problem Athanassenas [1]. The fluid is connected and the planes are simply connected inside any wetted regions Colter and Treinen [2]. The liquid forms a contact line along P_0 with contact angle γ_0. Plane P_H is at height $u(\ell) = H$, with its own contact line and contact angle γ_H. At planes P_0 and P_H are uniform solids that acts as boundary to the liquid volume.

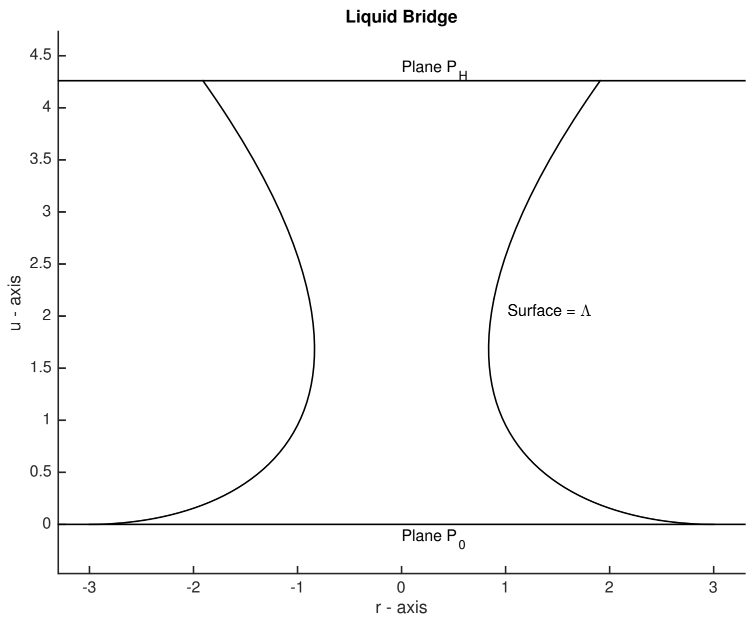

Figure V.1: A liquid bridge with boundaries P_0, P_H and the interfacial boundary Λ.

We prescribe some values on a generating curve (r, u) of a static liquid bridge:

- At arc length $s = 0$, the height is $u(0) = u_0$ with radius $r(0) = r_0$, and $\psi(0) = \psi_0$, and the contact angle is $\psi(0) = \gamma_0$.

- At arc length $s = \ell$, the height is $u(\ell) = H$ with radius $r(\ell) = r_H$, and $\psi(\ell) = \psi_H$, and the contact angle is $\psi(\ell) = \gamma_H$.

A solution to any static liquid bridge problem will have the initial and ending conditions listed below in equations (V.1) - (V.6) at $s = 0$ (left) and $s = \ell$ (right):

$$u(0) = 0 \qquad u(\ell) = H \tag{V.1}$$

$$V = V_0 \tag{V.2}$$

$$\psi(0) = \gamma_0 \qquad \psi(\ell) = \gamma_H, \tag{V.3}$$

or,

$$u(0) = 0 \qquad u(\ell) = H \tag{V.4}$$

$$V = V_0 \tag{V.5}$$

$$r(0) = r_0 \qquad r(\ell) = r_H. \tag{V.6}$$

Unlike in the sessile drop problem $\psi(s)$ can take any value in $[0, 2\pi]$. In our computation we account for this by subtracting π from the total angle of ψ, and in our graphs and charts when we display angles on the top plane P_H, we are using the internal angle, where $\psi(\ell) \subset [0, \pi]$.

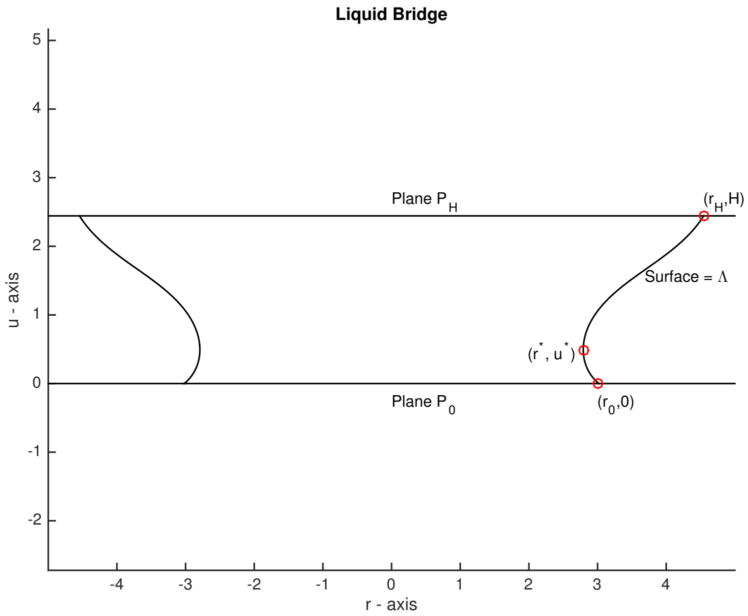

Figure V.2: A liquid bridge where r_0, r^*, r_H are marked.

The generating curves of the radially symmetric surface satisfy our previous three differential equations (I.4) - (I.6). Solving the system of equations with the initial and ending conditions, we derive the volume below.

Volume of a Liquid Bridge

THEOREM 3. *The volume of a liquid bridge connecting two horizontal planes seperated by distance H is*

$$V = \pi r^2 H - \frac{\pi}{\kappa}\left(2r_H \sin\psi_H - 2r_0 \sin\psi_0 - \lambda\left(r_H^2 - r_0^2\right)\right). \tag{V.7}$$

Proof. Let there be a volume of liquid between two planes separated by distance H. The volume integral is

$$V = \int_0^H \pi\rho^2\, du. \tag{V.8}$$

Since u is a function of arc length s, we note that the path from height $u = 0$ to $u = H$ is the path along surface Λ from arc length $s = 0$ to $s = \ell$. Because there is often concavity along Λ, we cannot easily integrate along the entire curve, and we must create regions along the surface that are either strictly monotonically increasing or strictly decreasing.

We do this by introducing an intermediate height u^* between planes P_0 and P_H. Define r_0 as the radial distance of the point on Λ, $(r_0, 0)$, where $s = 0$ and height $u(0) = 0$. Define r^* as the distance of point (r^*, u^*) where $0 < s < \ell$ and $\psi(s) = \pm\pi/2$. Define r_H as the distance of (r_H, u_H) where $s = \ell$ and $u(\ell) = H$. Since r is a function of s, then we can reorient the path along the curve according to the relative positions of r_0, r^*, and r_H. This gives four cases:

1. r^* is to the left of both r_0 and r_H
2. r^* is to the right of both r_0 and r_H
3. $r_0 < r^* < r_H$,
4. or $r_H < r^* < r_0$.

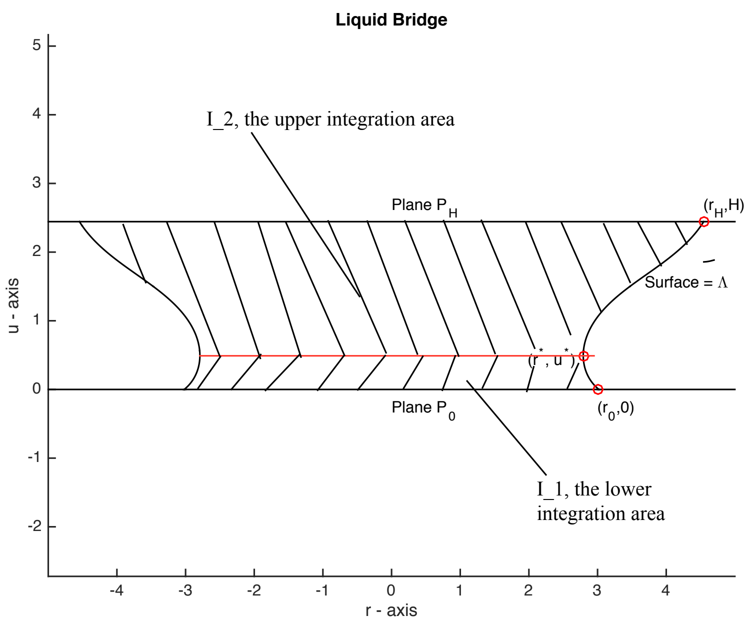

Figure V.3: A liquid bridge where r_0, r^*, r_H are marked, and the integration areas are highlighted, demonstrating the monotonic regions along the surface Λ, I_1 and 1_2.

We begin by integrating by parts over the two regions

$$\begin{aligned}
V &= \int_0^H \pi\rho^2\,du \\
&= \int_0^{u^*} \pi\rho^2\,du + \int_{u^*}^H \pi\rho^2\,du \\
&= \pi\rho^2 u|_{u=0}^{u^*} - 2\pi \int_{r*}^{r_0} \rho u\,d\rho + \pi\rho^2 u|_{u=u^*}^{H} - 2\pi \int_{r^*}^{r_H} \rho u\,d\rho \\
&= \pi\rho^2 H - 2\pi \left(\int_{r*}^{r_0} \rho u\,d\rho + \int_{r^*}^{r_H} \rho u\,d\rho \right).
\end{aligned}$$

Let I_1 be the integral from r^* to r_0, and let I_2 be the integral from r^* to r_H. Then the volume equation simplifies to

$$V = \pi r^2 H - 2\pi(I_1 + I_2). \tag{V.9}$$

Recall that by (I.6)

$$u = \frac{1}{\kappa}\left(\frac{d\psi}{ds} + \frac{\sin\psi}{\rho} - \lambda\right).$$

Evaluating I_1, gives that

$$\begin{aligned}
I_1 &= \int_{r*}^{r_0} \rho u\,d\rho \\
&= \frac{1}{\kappa}\int_{r*}^{r_0} \rho\left(\frac{d\psi}{ds} + \frac{\sin\psi}{\rho} - \lambda\right)\,d\rho \\
&= \frac{1}{\kappa}\left[\int_{r*}^{r_0} \rho\frac{d\psi}{ds}\,d\rho + \int_{r*}^{r_0} \sin\psi\,d\rho - \int_{r*}^{r_0} \lambda\rho\,d\rho\right].
\end{aligned} \tag{V.10}$$

Integrating the middle term by parts in (V.10) gives

$$\int \sin\psi\,d\rho = \rho\sin\psi - \int \rho\cos\psi\,d\psi. \tag{V.11}$$

So that

$$I_1 = \frac{1}{\kappa}\left[\int_{r^*}^{r_0} \rho \frac{d\psi}{ds}\, d\rho + \rho\sin\psi - \int_{\psi_0}^{-\frac{\pi}{2}} \rho\cos\psi\, d\psi - \int_{r*}^{r_0} \lambda\rho\, d\rho\right]$$

Here, we note that because of (I.4), $\cos\psi = dr/\, ds$

$$\begin{aligned}
I_1 &= \frac{1}{\kappa}\left[\int_{r^*}^{r_0} \rho \frac{d\psi}{ds}\, d\rho + \rho\sin\psi - \int_{\psi_0}^{-\frac{\pi}{2}} \rho \frac{d\rho}{ds}\, d\psi - \lambda\int_{r^*}^{r_0} \rho\, d\rho\right] \\
&= \frac{1}{\kappa}\left[\rho\sin\psi - \lambda\int_{r^*}^{r_0} \rho\, d\rho\right] \\
&= \frac{1}{\kappa}\left[\rho\sin\psi - \lambda\left(\frac{\rho^2}{2}\right)\right]_{r=0}^{r_0} \\
&= \left.\frac{2r\sin\psi - \lambda\, r^2}{2\kappa}\right|_{r=r^*}^{r_0}.
\end{aligned} \tag{V.12}$$

Evaluating I_2 is similar. In fact, it's the same integral up to the values for r. Since we are operating in *Case 1*, we can just replace the upper limit r_0 with r_H to get

$$\begin{aligned}
I_2 &= \int_{r*}^{H} \rho u\, d\rho \\
&= \frac{1}{\kappa}\int_{r*}^{r_0} \rho\left[\frac{d\psi}{ds} + \frac{\sin\psi}{\rho} - \lambda\right] d\rho \\
&= \frac{1}{\kappa}\left[\int_{r*}^{H} \rho \frac{d\psi}{ds}\, d\rho + \int_{r*}^{H} \sin\psi\, d\rho - \int_{r*}^{H} \lambda\rho\, d\rho\right] \\
&= \left.\frac{2r\sin\psi - \lambda\, r^2}{2\kappa}\right|_{r=r^*}^{H}.
\end{aligned} \tag{V.13}$$

Combining (V.12) and (V.13) we get the volume for Case 1 ($r_0 > r^*, r_H > r^*$) is

$$
\begin{aligned}
V &= \pi r^2 H - 2\pi(I_1 + I_2) \\
&= \pi r^2 H - 2\pi \left(\left[\frac{2r\sin\psi - \lambda\, r^2}{2\kappa} \right]_{r=r^*}^{r_0} + \left[\frac{2r\sin\psi - \lambda\, r^2}{2\kappa} \right]_{r=r^*}^{H} \right) \\
&= \pi r^2 H - 2\pi/2\kappa([-(2r_0 \sin\psi_0 - \lambda r_0 - (2r^* \sin\psi^* - \lambda r^*)) \\
&\qquad + 2r_H \sin\psi_H - \lambda r_H - (2r^* \sin\psi^* - \lambda r^*)]) \\
&= \pi r^2 H - \pi/\kappa \left(2r_H \sin\psi_H - 2r_0 \sin\psi_0 - \lambda(r_H^2 - r_0^2) \right)
\end{aligned}
$$

We will use the convention that because $r^* < r_0$ while $u^* > u_0$ we must use a negative sign in the evaluation of the integral. This is because the path is now vertically downward along the generative curve. We use that convention when necessary in each case.

The general solution (irrespective of case) for integrals I_1 and I_2, demonstrated in Fig. V.3 are identical up to endpoints. But for a proof we must consider the relative locations of the endpoints, which are shown here

$$
I_1 = \left. \frac{2r\sin\psi - \lambda\, r^2}{2\kappa} \right|_{r=r_1}^{r_2} \qquad I_2 = \left. \frac{2r\sin\psi - \lambda\, r^2}{2\kappa} \right|_{r=r_3}^{r_4},
$$

where in I_1 the lower limit r_1 is simply the leftmost radius of r_0 and r^*, and the upper limit r_2 is the rightmost radius. Similarly, for integral I_2, we choose the lower limit r_3 to be the leftmost between r_H and r^*, and for the upper limit r_4 we choose the rightmost radius. (Note that the limits of integration $\{r_1, r_2, r_3, r_4\}$ are all irrespective of arc length s. Whereas r_0 and r_H are located at $s = 0$ and $s = \ell$, respectively, while r^* is located at s^*, where $0 < s^* < \ell$.)

Then the general volume formula is given by

$$
\begin{aligned}
V &= \pi r^2 H - 2\pi(I_1 + I_2) \\
&= \pi r^2 H - \frac{\pi}{\kappa} \left[(2r\sin\psi - \lambda\, r^2)\Big|_{r=r_1}^{r_2} + (2r\sin\psi - \lambda\, r^2)\Big|_{r=r_3}^{r_4}) \right],
\end{aligned}
$$

The integrals are solved for each case below:

Case 1 ($r^* < r_0$ and $r^* < r_H$), which was shown previously, is the case where both r_0 and r_H are greater than r^*. However, it is not determined whether $r_0 \geq r_H$ or $r_0 \leq r_H$. Again, notice that we use the convention of a negative sign in the expression to denote a downward path along the curve.

$$
\begin{aligned}
V &= \pi r^2 H - \pi/\kappa \left[-\left(2r\sin\psi - \lambda\ r^2\right)\Big|_{r=r^*}^{r_0} + \left(2r\sin\psi - \lambda\ r^2\right)\Big|_{r=r^*}^{r_H} \right] \\
&= \pi r^2 H - \pi/\kappa[-(2r_0\sin\psi_0 - \lambda r_0^2 - (2r^*\sin\psi^* - \lambda r^{*2})) \\
&\qquad + 2r_H\sin\psi_H - \lambda r_H^2 - (2r^*\sin\psi^* - \lambda r^{*2})] \\
&= \pi r^2 H - \pi/\kappa\left[2r_H\sin\psi_H - 2r_0\sin\psi_0 - \lambda\left(r_H^2 - r_0^2\right)\right]
\end{aligned}
$$

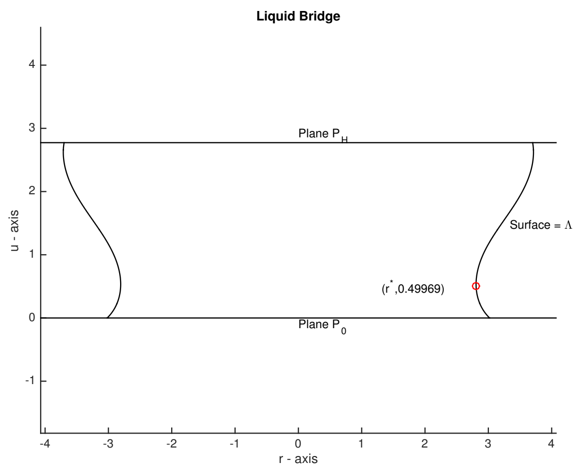

Figure V.4: Case 1: A liquid bridge drop where r^* is the left of both r_0 and r_H.

Case 2 ($r_0 > r^* > r_H$) can be thought of as a curved diagonal surface. We have

$$
\begin{aligned}
V &= \pi r^2 H - \pi/\kappa[-(2r_0\sin\psi_0 - \lambda r_0^2 - (2r^*\sin\psi^* - \lambda r^{*2})) \\
&\qquad - (2r^*\sin\psi^* - \lambda r^{*2} - (2r_H\sin\psi_H - \lambda r_H^2))] \\
&= \pi r^2 H - \pi/\kappa\left[2r_H\sin\psi_H - 2r_0\sin\psi_0 - \lambda\left(r_H^2 - r_0^2\right)\right]
\end{aligned}
$$

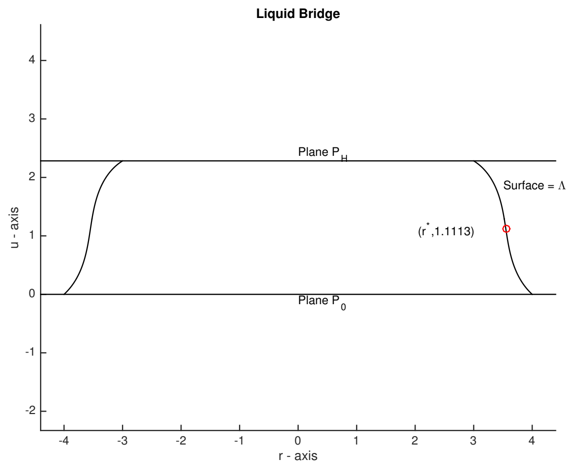

Figure V.5: Case 2: A liquid bridge drop where r^* is in between r_0 and r_H, and $r_0 > r_H$.

Case 3 $(r_H > r^* > r_0)$ is when the relative positions of r_0 and r_H are reversed from Case 2 so that now $r_0 > r^* > r_H$. We have

$$\begin{aligned} V &= \pi r^2 H - \pi/\kappa[2r^* \sin\psi^* - \lambda r^{*2} - (2r_0 \sin\psi_0 - \lambda r_0^2) \\ &\quad + 2r_H \sin\psi_H - \lambda r_H^2 + (2r^* \sin\psi^* - \lambda r^{*2})] \\ &= \pi r^2 H - \pi/\kappa \left[2r_H \sin\psi_H - 2r_0 \sin\psi_0 - \lambda\left(r_H^2 - r_0^2\right)\right] \end{aligned}$$

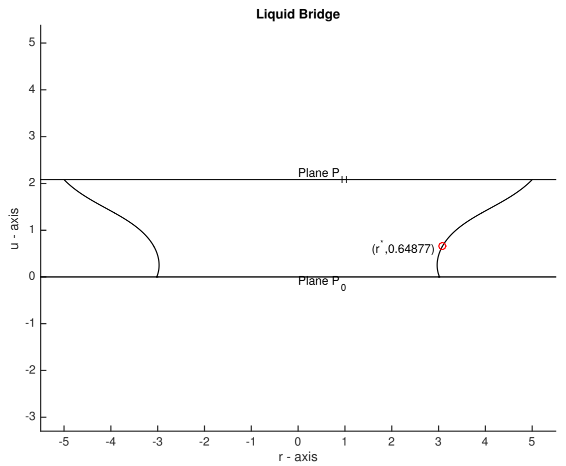

Figure V.6: Case 3: A liquid bridge drop where r^* is in between r_0 and r_H, and $r_0 < r_H$.

Case 4 $(r_0 < r^*$ and $r_H < r^*)$ is the reversal of Case 1, and both r_0 and r_H are both less than r^*. We have

$$V = \pi r^2 H - \pi/\kappa[2r^* \sin\psi^* - \lambda r^{*2} - (2r_0 \sin\psi_0 - \lambda r_0^2)$$
$$- (2r^* \sin\psi^* - \lambda r^{*2} - (2r_H \sin\psi_H - \lambda r_H^2))]$$
$$V = \pi r^2 H - \pi/\kappa \left[2r_H \sin\psi_H - 2r_0 \sin\psi_0 - \lambda \left(r_H^2 - r_0^2\right)\right]$$

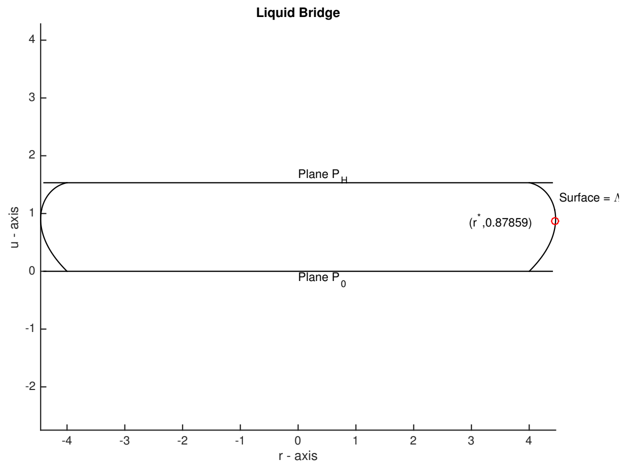

Figure V.7: Case 4: A liquid bridge drop where r^* is to right of both r_0 and r_H.

$\therefore$ All cases give the same solution. Therefore, we derive the volume of the symmetrical liquid bridge

$$V = \pi r^2 H - \frac{\pi}{\kappa}\Big(2r_H \sin\psi_H - 2r_0 \sin\psi_0 - \lambda \left(r_H^2 - r_0^2\right)\Big). \tag{V.14}$$

□

Numerical Solver

The solution curves for the static liquid bridge are generated in a similar manner as the static sessile problem. We integrate our system of differential equations (I.4) - (I.6) and use FSOLVE and ODE45 to adjust the values of a guess vector, **guess**, until we solve for our ending criteria. We have two sets of initial conditions for the liquid bridge. The first initial conditions are the known contact angles on each plane, γ_0 and γ_H, and then the radii r_0 and r_H are unknown. Then FSOLVE adjusts the values in **guess** $= \langle r_0, \ell, \lambda \rangle$. The new ending criteria are then given by the following:

$$V(\ell) - V = 0 \tag{V.15}$$

$$u(\ell) - H = 0 \tag{V.16}$$

$$\psi(\ell) - \psi_H = 0. \tag{V.17}$$

VI. THE DYNAMIC LIQUID BRIDGE

Using similar techniques to calculate contact line velocity that we used in the dynamic sessile drop problem, we find equilibrium positions for endpoints (r, u) at $(r_0, 0)$ and (r_H, H). We also find the intermediate (non-equilibrium) values for ψ_0 and ψ_H using similar MATLAB codes with the same starting and stopping conditions as the stationary problem. The main difference is that for the dynamic bridge, there is a smaller range of solutions. For a given r_0 and r_H, there will only be a few solutions for the contact angles γ_0 and γ_H on each plane, and we see that the solutions are not as robust as the sessile drop. This dependence makes finding solutions rare. However, with careful selection of parameters we can find a solution for the variable volume problem. Again, for this chapter $\kappa_S = 1$ and we assume constant friction over the solid/liquid interface.

Calculating contact velocity along two surfaces

We again implement an Euler method to solve for the radius, and we need to prescribe radius in our ending condition, giving the dynamic ending conditions as

$$V - V_0 = 0, \tag{VI.1}$$

$$u(\ell) - H = 0, \tag{VI.2}$$

$$r(\ell) - r_H = 0, \tag{VI.3}$$

In the dynamic liquid bridge problem there are two contact lines curves. The liquid bridge surface satisfies our system of ODEs, (I.4) - (I.6). Thus, the velocities can be solved with the same methods as the sessile drop, and the boundary value problem is solved as one system with ODE45 and FSOLVE. In this case we use a reasonable guess for our unknowns: arc length ℓ, lower contact angle $\psi(0)$, and Lagrange multiplier λ. Employing the same convention for contact line velocity as with the dynamic sessile drop, the velocity for each contact line $v = \dot{r}(u,t)$, where either $u = 0$ or $u = H$.

$$v = \kappa_S(u)[\psi(u,t) - \gamma(u)]^3 \tag{VI.4}$$

On the lower plane, where $u = 0$, the radius function $r(0,t)$ is

$$
\begin{aligned}
r(0,t) &= (\Delta t)[v(\psi(0,t), \kappa_S(0), \gamma)], && \text{(VI.5)}\\
&= (\Delta t)\kappa_S(0)(\psi(0,t)^2 - \gamma^2). && \text{(VI.6)}
\end{aligned}
$$

On the upper plane, where $u = H$, the radius function $r(H,t)$ is

$$
\begin{aligned}
r(H,t) &= (\Delta t)[v(\psi(H,t), \kappa_S(H), \gamma)], && \text{(VI.7)}\\
&= (\Delta t)\kappa_S(H)(\psi(H,t)^2 - \gamma^2). && \text{(VI.8)}
\end{aligned}
$$

The mechanics along the top and bottom planes are considered the same as for the plane beneath a sessile drop, as mentioned in the considerations of a the solid at P_0 and P_H. So, we expect contact line behaviors in the liquid bridge similar to the sessile drop case, shown in Fig. VI.1 and Fig. VI.2. However, because the entire curve Λ is connected to two independent planes there will be an fewer solutions where velocity remains smooth. These simulations do not always begin with a physically relevant configuration. Consequently, they are at times numerically unstable.

Similar to the sessile drop, we expect with constant and slowly changing volume that our system will achieve equilibrium if we are within our solvable range for $\psi(s)$. We see that with reasonable guesses, because of our robust solver, that the radius will shift with predictable velocity over time, and eventually $\psi(0) \to \gamma_0$

and $\psi(\ell) \to \gamma_H$. We see this trend in the figures below.

We ran simulations where t is 1 second. $\psi(0)$ and $\psi(\ell)$ took values between 0 and π, evenly spaced, with intervals of $\pi/14$, so that there are 15×15 inputs on gamma. Top and bottom plane radius is an input, where $r(0, H) \in [4, 4.5, 5]$. We set initial volume $V_0 = 90$ and height $u_H = H = 2$. Under these configurations the liquid bridge simulations produced viable results, when $\lambda \approx -0.5$ in **guess**. Note: We define our variable volume functions in Appendix B.

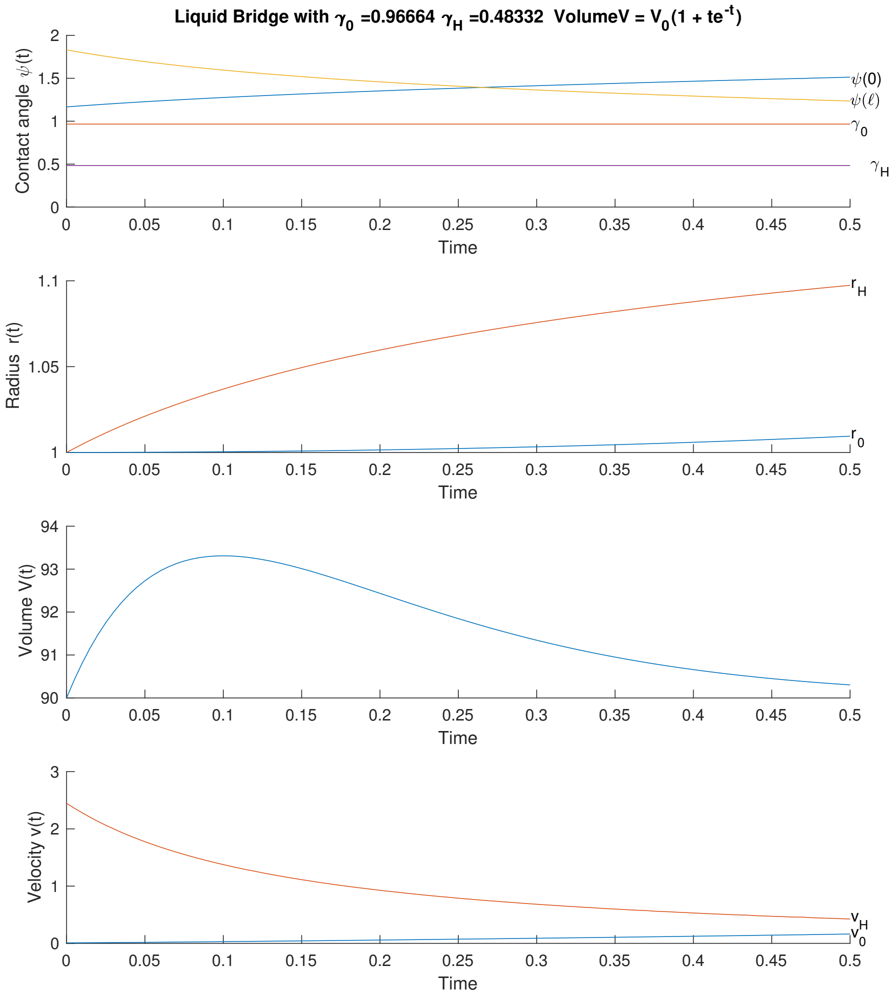

Figure VI.1: Graph showing behavior on the two contact lines of a liquid bridge $t = 0.5$ with exponential volume function. $\psi(\ell)$ is tending towards γ_H as v_H goes to zero.

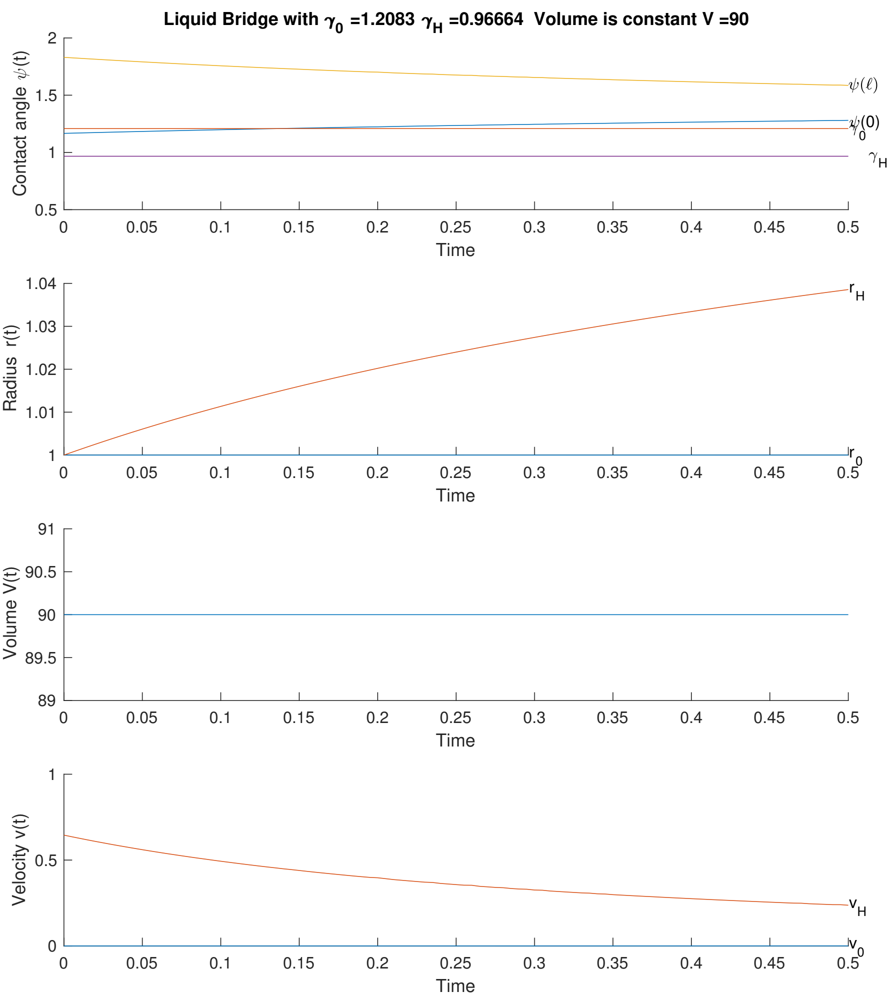

Figure VI.2: Graph showing behavior on the two contact lines of a liquid bridge $t = 0.5$ seconds with constant volume. $\psi(\ell)$ is goes towards γ_H as v_H goes to zero.

Receding and advancing angles along two contact lines

When considering advancing and receding angles, our velocity function is fundamentally different. The $v = \kappa_S \cdot f(|\nabla u|^k - 1)$ model, where $k = 2, 3$, is replaced with the piecewise function below. Note that for the liquid bridge, we denote which contact curve is being acted upon by a comma-demarcated sub-index. Also, we choose the cubed velocity equation once again, and contact velocity along the bottom plane is given by

$$v(t) = \begin{cases} -\kappa_S[\psi(0) - \theta_{R,0}]^3 & \psi(0) > \theta_{R,0} \\ 0 & \theta_{R,0} \leq \psi(0) \leq \theta_{A,0} \\ \kappa_S[\psi(0) - \theta_{A,0}]^3 & \psi(0) > \theta_{A,0}, \end{cases} \tag{VI.9}$$

while the contact velocity along the top plane

$$v(t) = \begin{cases} -\kappa_S[\psi(\ell) - \theta_{R,H}]^3 & \psi(\ell) > \theta_{R,H} \\ 0 & \theta_{R,H} \leq \psi(\ell) \leq \theta_{A,H} \\ \kappa_S[\psi(\ell) - \theta_{A,H}]^3 & \psi(\ell) > \theta_{A,H}. \end{cases} \tag{VI.10}$$

The velocity function acts independently on each contact line similarly to the velocities in previous chapter, dependent only on $\psi(0, \ell)$ and the arbitrary constants θ_A and θ_R. The friction function $\kappa_S = 1$. What we expect from this is that the velocity behaves normally, which is to slowly shrink to zero when volume is slowly changing, until the $\theta_{A,H}$ threshold is crossed (seen in Fig. VI.3 and Fig. VI.4), where either $\theta_{A,0} \leq \gamma_0 \leq \theta_{R,0}$ or $\theta_{A,H} \leq \gamma_H \leq \theta_{R,H}$ and velocity is frozen at zero for either contact line. Consequently, the radius remains unchanged until a contact angle leaves the hysteresis region, where $\psi(0) \in [\theta_{A,0}, \theta_{R,H}]$ and $\psi(\ell) \in [\theta_{A,H}, \theta_{R,H}]$.

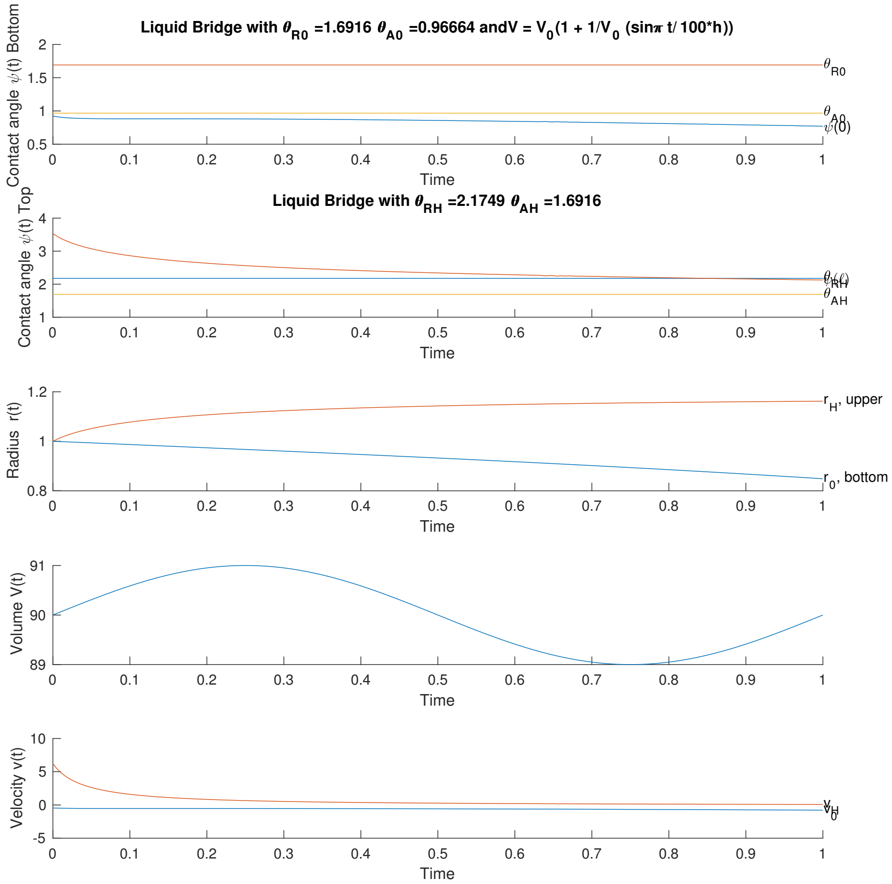

Figure VI.3: A sinusoidal volume shows quicks movement of the contact angle θ_H towards γ_H as velocity v_H goes to zero.

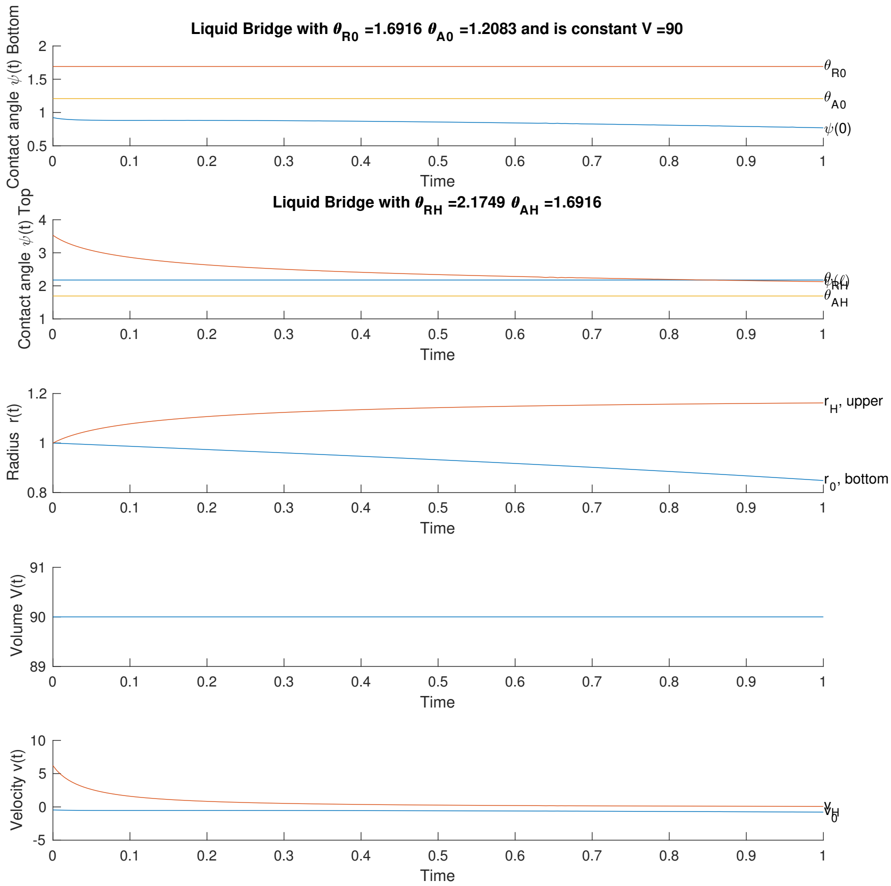

Figure VI.4: A constant volume shows asymptotic behavior of the contact angle θ_H as velocity v_H goes to zero.

VII. CONCLUSIONS FOR LIQUID BRIDGES

There is noticeable decrease in the amount of dynamic liquid bridges configurations that are stable, and even fewer that tend towards equilibrium, compared to the sessile drop model. The stability of the dynamic liquid bridge is a problem that by itself warrants more study. Within the scope of this investigation, the problem came down to optimization of our inputs. The guesses, which include the unknowns and the prescribed radii needed to be closely tailored to the volume. During this study, the parameters needed to be changed until a configuration worked consistently for a given volume, which was $\mathcal{V} = 90$. One consistent example of a failing configuration occurred when contact angles $\gamma_0 = \gamma_H$. Having the same contact angles on both planes is rare except when $\gamma_0 = \gamma_H = \pi/2$, which [9] asserts should produce a stable liquid bridge in the static model when volume is large enough, specifically when $\mathcal{V} > H^3/\pi$. This is an example of a cylindrical liquid bridge, which Colter and Treinen [2] studied, from which the numerical methods and model are adapted to this paper. There are however many stable solutions when the radii $r_0 = r_H$ and $\psi(\ell) \neq \psi(0)$, when the volume is appropriate.

In the liquid bridge we see less volume function dependence. This is likely due to the decrease in degrees of freedom in the liquid bridge problem compared to the sessile drop problem. For instance both radii and the height needed are inputs for the dynamic liquid bridge. Since we choose r_0, r_H, $\mathcal{V}$, $u_0 = 0$, $u_H = H$, and $\kappa_S = 1$, this leaves only $\psi(s)$ and λ as free parameters. Whereas in the sessile drop we only predetermine r_0 and $\mathcal{V}$, leaving ℓ, $\lambda = u(\ell)$, and $\psi(s)$ as free parameters. The liquid bridge is a much bigger problem, and solving the system of differential equations outputs less information and requires much more information. It is highly dependent upon initial conditions to find solutions. Although there is a theorem, which says a liquid bridge between two planes of a certain height must exist for some volume, given by [1], we have need a physically viable configuration in the initial values.

Because of the dependence upon initial values, no configuration produced a stable liquid bridge exists for many initial values of the parameters. For instance when when $V_0 = 90$ and $\gamma_0 \geq 1.6916$ there are no solutions, but there are many solutions when $V_0 = 90$ and $\gamma_H \geq 1.6916$, altogether this is demonstrated in Fig. VII.1 - Fig. VII.3. This behavior may suggest something like an upper limit to an equilibrium range for this volume and height with initial radii $r_0 = 4, r_H = 4$. However, it would be presumptuous to suggest that there an equilibrium range for the liquid bridge exists in our model due to its dependence on both $\psi(0)$ and $\psi(\ell)$.

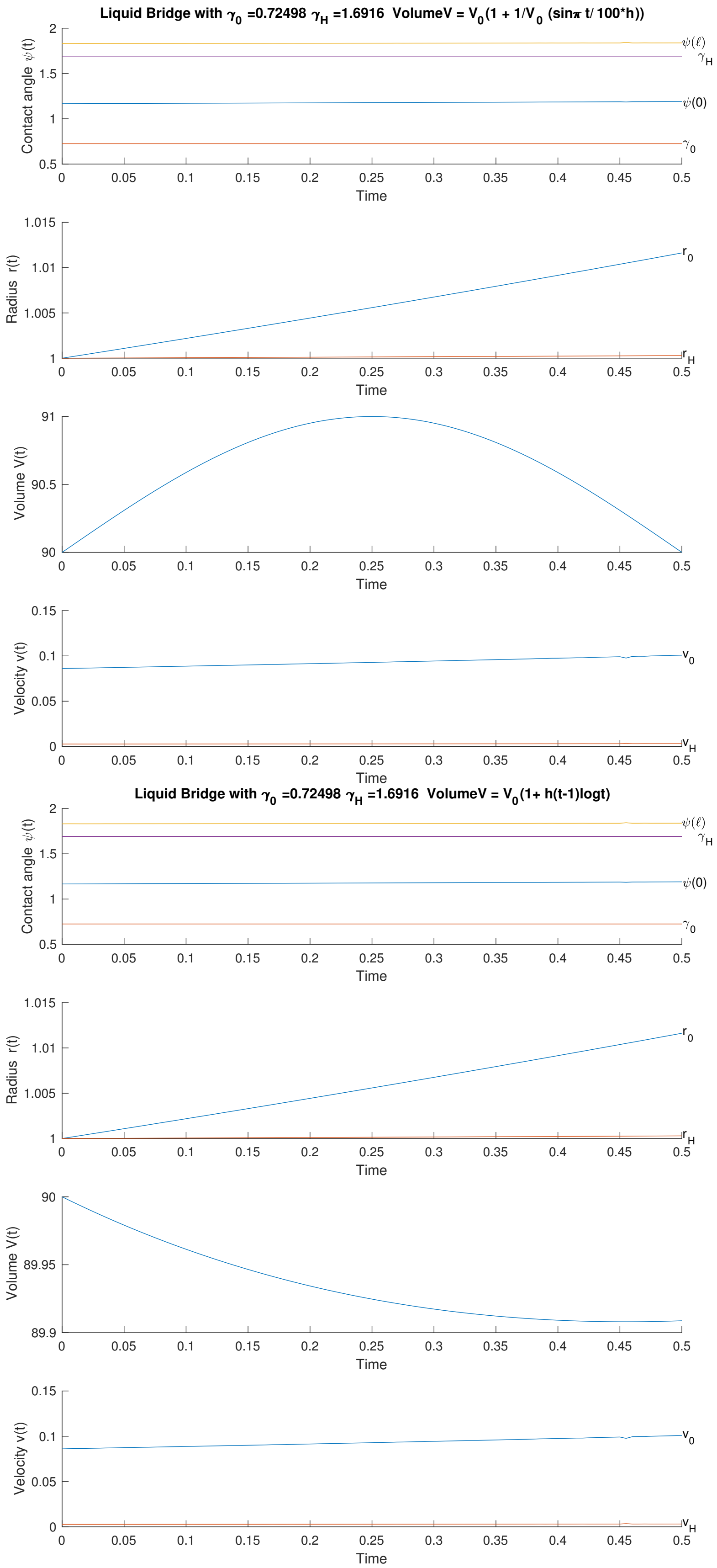

Figure VII.1: Two liquid bridges with $\gamma_H = 1.6916$ (on the top plane) and sinusoidal and logarithmic volumes functions and $\gamma_0 = 0.72498$.

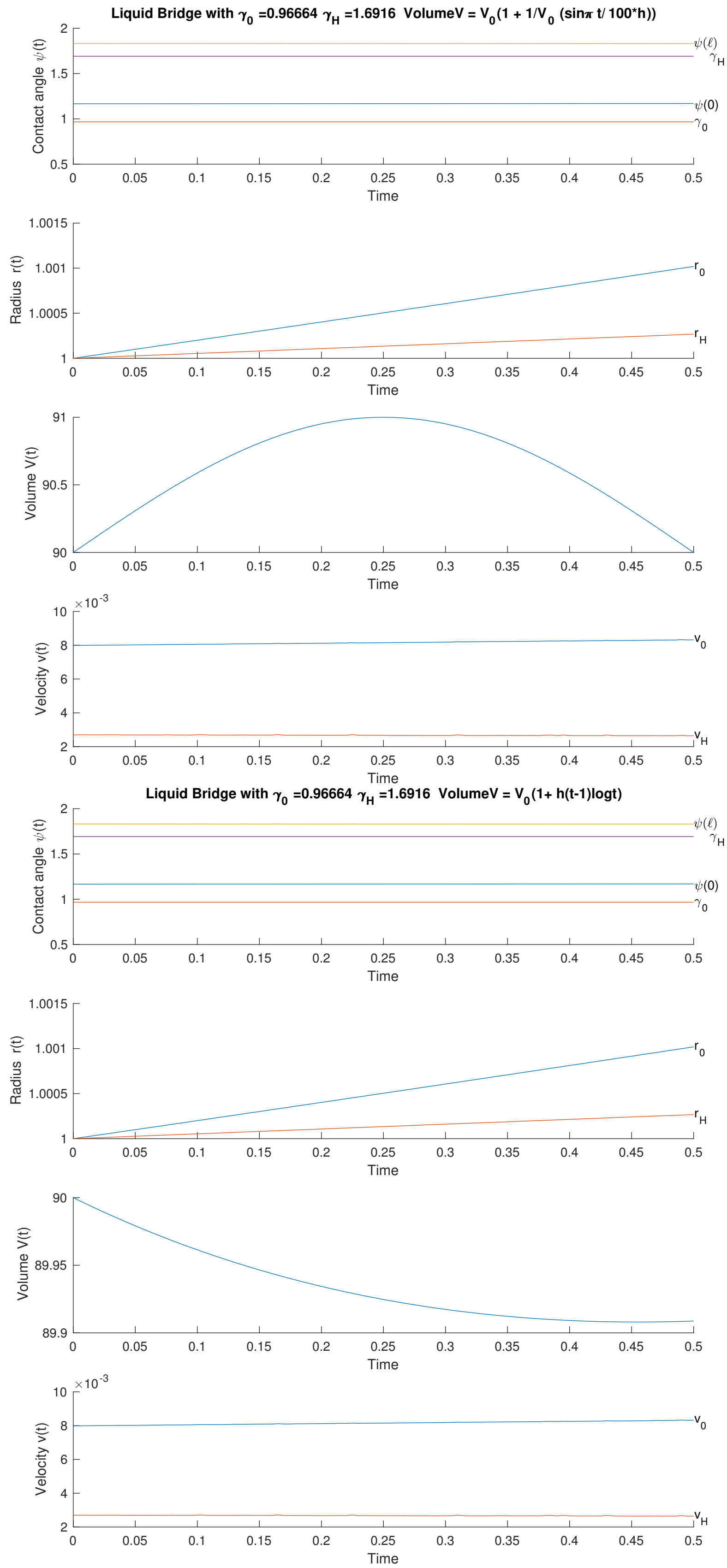

Figure VII.2: Two liquid bridges with $\gamma_H = 1.6916$ (on the top plane) and sinusoidal and logarithmic volumes functions and $\gamma_0 = 0.96664$.

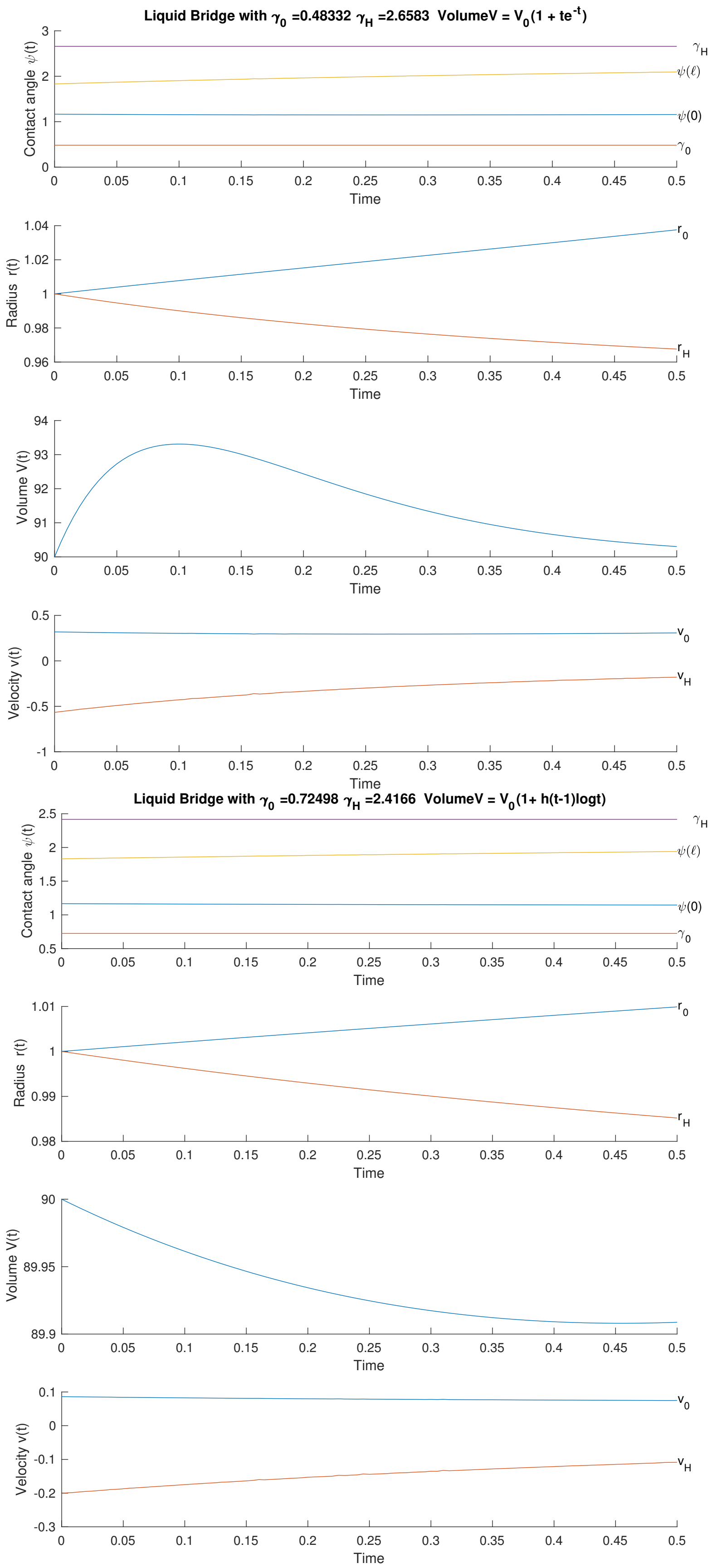

Figure VII.3: Two liquid bridges with solutions. $\gamma_H > 1.6916$ (on the top plane) with $\gamma_0 < 1.6916$.

Exploring the optimization of initial conditions and guesses, we saw that using a highly discretized set of γ's, θ's, and **guess** values left gaps in the data. Finn and Shinbrot suggest that the hysteresis of the angles, $\theta_A - \theta_R$, would be spread agross a continuous range of contact angles, where given a r_0 and r_H the liquid bridge should have stable solutions [4]. In fact it was difficult to find solutions when any parameter was changed in **guess** $= \langle \ell, u_0, \lambda \rangle$.
Altogether, while the liquid bridge problem relied heavily upon initial conditions, it remain a problem solvable when given enough volume and flexibility in the guesses. Particularly troublesome was the Lagrange multiplier λ in the range of radii, in which were solvable when $V_0 = 90$. λ needed to be exactly -0.5. This was unexpected because **guess** is just an initial value, and we employ a shooting method, which runs through all nearby possible values to find a solution. For instance ℓ could take on different values. We looked specifically at $\ell = 1, 1.5, 2$, and for the liquid bridge problem $\ell = 2$ was the default. Arc length $\ell = 1$ showed no solutions, and $\ell = 1.5$ showed a limited range of solutions. $\ell = 1$ showed no solutions, whereas $\ell = 1.5$ showed a different set of contact angles, for which velocities tended towards equilibrium, than $\ell = 2$.

APPENDIX SECTION

APPENDIX A

Algorithms

Algorithm 1 Sessile Drop Generator Algorithm

```
Choose guess vector values for unknowns, guess = ⟨u_0, ℓ, λ⟩
Run Capillary_ODE_Solver(u_0, ℓ, λ)
Choose volume V
run ODE45 from s = 0 to s = ℓ return vector out = ⟨u, r, ψ⟩
repeat
    FSOLVE to solve a residual function ResFun(u_0, ℓ, λ)
    open ODE45 from s = 0 to s = ℓ return vector out = ⟨u, r, ψ⟩
    ℓ = length(out)
    V = πr(ℓ)^2 u(0) − (2πr(ℓ)/κ)(sin ψ(ℓ) + πr(0)^2)
```

$$
\begin{aligned}
&\text{ResFun}\\
V - V(0) &= 0\\
r(\ell) - r(0) &= 0\\
u_0 - \lambda(0) &= 0
\end{aligned}
$$

```
until ResFun is minimized
close
```

Algorithm 2 Sessile Drop Contact Line Velocity

```
Choose reasonable guess for r(0, 0)
loop:
for i = 0, 1, 2, 3... do
    Solve for r(i)
    v_i = κ_S[ψ(i) − γ]^3
    r(i + 1) = r(i) + Δt_j v_0(i)
end
close
```

Algorithm 3 Liquid Bridge Generator Algorithm

Choose guess vector values for unknowns, $guess = \langle r_0, \ell, \lambda \rangle$
Run Capillary_ODE_Solver(r_0, ℓ, λ)
Choose volume V
run ODE45 from $s = 0$ to $s = \ell$ **return** vector $out = \langle u, r, psi \rangle$
repeat
    FSOLVE to solve a residual function ResFun(r_0, ℓ, λ)
    open ODE45 from $s = 0$ to $s = \ell$ **return** vector $out = \langle u, r, \psi \rangle$
    $\ell = \text{length}(out)$
    $V = \pi r(\ell)^2 u(0) - (\pi/\kappa)\Big[2 \sin\psi(0) r(0) + 2 \sin\psi(\ell) - \lambda\pi\Big(r(\ell) - r(0)^2\Big)\Big]$

$$
\begin{aligned}
&\text{ResFun} \\
V(\ell) - V &= 0 \\
u(\ell) - H &= 0 \\
\psi(\ell) - \psi_H &= 0
\end{aligned}
$$

until ResFun is minimized
close

Algorithm 4 Liquid Bridge Contact Lines Velocities

Choose reasonable guess for r_0
Choose reasonable guess for r_H
loop:
for $i = 0, 1, 2, 3...$ **do**
    Solve for $\{r_0(i), r_H(i)\}$
    $v_0(i) = \kappa_S[\psi_0(i)^3 - \gamma_0^3]$
    $v_0(i) = \kappa_S[\psi_H(i)^3 - \gamma_0^3]$
    $r_0(i+1) = r_0(i) + \Delta t_i v_0(i)$
    $r_H(i+1) = r_H(i) + \Delta t_i v_H(i)$
end
close

REFERENCES

[1] Athanassenas, M. (1992). A free boundary problem for capillary surfaces. *manuscripta mathematica*, 76(1):5–19.

[2] Colter, L. and Treinen, R. (2015). Cylindrical liquid bridges. *Involve*, 8(4):695–705.

[3] Finn, R. (1986). *Equilibrium Capillary Surfaces*. Number 284 in Grundlehren der mathematischen Wissenschaften: A Series of Comprehensive Studies in Mathematics. Springer-Verlag New York Inc.

[4] Finn, R. and Shinbrot, M. (1987). The capillary contact angle i. the horizontal plane and stick-slip motion. *Journal of Mathematical Analysis and Applications*, 123(1):1–17.

[5] Greenspan, H. P. (1978). On the motion of a small viscous droplet that wets a surface. *Journal of Fluid Mechanics*, 84:125–143.

[6] Guidotti, P. (2013). Equilibria and Their Stability for a Viscous Droplet Model. *ArXiv e-prints*.

[7] Huh, C. and Scriven, L. E. (1971). Hydrodynamic model of steady movement of a solid/liquid/fluid contact line. *Journal of colloid and interface science*, 35(1):85–101.

[8] Neogi, P. and Miller, C. A. (1983). Spreading kinetics of a drop on a rough solid surface. *Journal of Colloid and Interface Science*, 92(2):338 – 349.

[9] Vogel, T. I. (1987). Stability of a drop trapped between two parallel planes: Preliminary report. In Concus, P. and Finn, R., editors, *Variational Methods for Free Surface Interfaces*, pages 139–144. Springer New York.

[10] Wente, H. C. (1980). The symmetry of sessile and pendent drops. *Pacific J. Math.*, 88(2):387–397.